# The MJO-QBO Relationship in a GCM with Stratospheric Nudging

ZANE MARTIN, a CLARA ORBE, b SHUGUANG WANG, c AND ADAM SOBEL c,d

a Department of Atmospheric Science, Colorado State University, Fort Collins, Colorado <sup>b</sup> NASA Goddard Institute for Space Studies, New York, New York <sup>c</sup> Department of Applied Physics and Applied Mathematics, Columbia University, New York, New York d Lamont-Doherty Earth Observatory of Columbia University, Palisades, New York

(Manuscript received 10 August 2020, in final form 23 February 2021)

ABSTRACT: Observational studies show a strong connection between the intraseasonal Madden-Julian oscillation (MJO) and the stratospheric quasi-biennial oscillation (QBO): the boreal winter MJO is stronger, more predictable, and has different teleconnections when the QBO in the lower stratosphere is easterly versus westerly. Despite the strength of the observed connection, global climate models do not produce an MJO-QBO link. Here the authors use a current-generation ocean-atmosphere coupled NASA Goddard Institute for Space Studies global climate model (Model E2.1) to examine the MJO-QBO link. To represent the QBO with minimal bias, the model zonal-mean stratospheric zonal and meridional winds are relaxed to reanalysis fields from 1980 to 2017. The model troposphere, including the MJO, is allowed to freely evolve. The model with stratospheric nudging captures QBO signals well, including QBO temperature anomalies. However, an ensemble of nudged simulations still lacks an MJO-QBO connection.

KEYWORDS: Madden-Julian oscillation; Quasibiennial oscillation; Stratosphere-troposphere coupling; General circulation models

#### 1. Introduction

The intraseasonal Madden-Julian oscillation (MJO) and the stratospheric quasi-biennial oscillation (QBO) are two key modes of variability in the tropical atmosphere. The MJO is a planetary-scale, eastward propagating phenomena in which circulation and convection are coupled on ~30-60day time scales (Madden and Julian 1971, 1972; Zhang 2005; Jiang et al. 2020). MJO convection and circulation signals, which are mainly tropospheric, extend from the Indian Ocean through the west Pacific, although through teleconnections the MJO has global impacts (e.g., Stan et al. 2017) and is a key source of subseasonal-to-seasonal (S2S) predictability (e.g., Vitart 2017).

The quasi-biennial oscillation is a reversal of the tropical stratospheric zonal winds, alternating between easterly (QBOE) and westerly (QBOW) regimes with an approximately 28-month period (Baldwin et al. 2001). QBO transitions begin in the upper stratosphere and descend over time, driven by a spectrum of upward propagating tropical waves (Lindzen and Holton 1968; Holton and Lindzen 1972). Through thermal wind balance, QBO zonal winds are associated with temperature anomalies on the order of 1-2 K: lower stratospheric easterlies are accompanied by cold anomalies, and westerly periods have warm anomalies. Consistent with thermal wind balance, these temperature anomalies peak lower than corresponding wind anomalies, such that while wind signals extend down to approximately 70 hPa, temperature anomalies extend below this into the tropical tropopause layer.

Recent studies discovered a strong link between the MJO and the QBO during boreal winter: the MJO is more active, more

predictable, and displays different teleconnections in QBOE versus QBOW (Yoo and Son 2016; Son et al. 2017; Marshall et al. 2017). This MJO-QBO connection has been confirmed and its properties described further in many observational studies (Nishimoto and Yoden 2017; Hood 2017; Zhang and Zhang 2018; Densmore et al. 2019; Hendon and Abhik 2018; Abhik et al. 2019; Klotzbach et al. 2019; Mundhenk et al. 2018; Mayer and Barnes 2020; Hera Kim et al. 2020; Sakaeda et al. 2020) and in modeling works (Lee and Klingaman 2018; Abhik and Hendon 2019; Martin et al. 2019; Lim et al. 2019; Wang et al. 2019; Hyemi Kim et al. 2020; Martin et al. 2020; Toms et al. 2020; Lim and Son 2020). This literature confirms that the MJO-QBO connection is statistically robust in boreal winter, although not in other seasons. Other studies have revealed that the QBO does not strongly affect other types of tropical waves aside from the MJO (Abhik et al. 2019; Sakaeda et al. 2020) and the MJO-QBO connection has only emerged in recent decades (Klotzbach et al. 2019; Sakaeda et al. 2020).

Neither the intriguing features described above nor the root causes of the MJO-QBO link have been explained. In particular, climate models have struggled to show a realistic MJO-QBO connection, hampering understanding (Lee and Klingaman 2018; Hyemi Kim et al. 2020; Lim and Son 2020). This deficiency poses a major obstacle to understanding the MJO-QBO link: at a minimum, assuming the models are wrong in failing to reproduce the connection, this failure renders them inadequate tools to test hypothesized mechanisms of the observed connection. On the other hand, if the models are correct, it implies that the observed connection is a statistical fluke, despite the stringent tests it has passed indicating otherwise.

Some of the most promising modeling studies on MJO-QBO interactions have used forecast models cast as initial value problems, such as those participating in the S2S Prediction Project (Vitart et al. 2017). These models do in fact

Corresponding author: Zane Martin, zkmartin@rams.colostate.edu

show an MJO-QBO link in their ensembles of initialized forecast runs (Marshall et al. 2017; Abhik and Hendon 2019; Lim et al. 2019; Wang et al. 2019; Kim et al. 2019; Martin et al. 2020). However, it is difficult in those runs to separate the effect of each model's QBO on its MJO from the effect of the initial conditions, which already contain the observed MJO-QBO connection. It is not clear whether forecast models show an emergent MJO-QBO link, involving an actual QBO impact on the troposphere exerted within the model simulations themselves. Studies attempting to isolate the QBO's direct impact have not found a strong connection to the MJO: one study found a weaker-than-observed MJO-QBO relationship (Abhik and Hendon 2019), while others have concluded that none is present (Wang et al. 2019; Kim et al. 2019; Martin et al. 2020). This makes it difficult to use forecast models to examine the mechanisms connecting the MJO and the QBO.

Another approach is to use a free-running general circulation model (GCM), where the MJO is not tied to initial conditions. However, no known GCM has been shown to produce an MJO–QBO link once initial conditions are forgotten. Lee and Klingaman (2018) found that a GCM with an internally generated QBO displayed no relationship between the model's QBO and MJO across three 25-yr simulations. Hyemi Kim et al. (2020) and Lim and Son (2020) looked across, respectively, the CMIP6 and CMIP5 models (Eyring et al. 2016), and showed that among those models that satisfied certain criteria for simulating the QBO and the MJO, none had a strong and clear MJO–QBO link.

A common issue noted in these studies is the presence of GCM biases in QBO signals in the upper troposphere and lower stratosphere (UTLS; Richter et al. 2020). In particular, the magnitude of the cold anomalies during QBOE and the warm anomalies during QBOW are too weak in models, and QBO temperature changes in the UTLS are therefore too small. Lee and Klingaman (2018), Hyemi Kim et al. (2020), and Lim and Son (2020) (among others) proposed that these QBO temperature biases might explain why GCMs lack an MJO–QBO connection. Equally possible, though less discussed or diagnosed in this literature, is that MJO biases may contribute to the lack of a signal, as discussed more below.

More generally, these QBO temperature anomalies have garnered attention as a viable path through which the QBO could alter the MJO, perhaps by allowing deep convection to penetrate higher and more vigorously into the tropopause when the UTLS is cold (Collimore et al. 2003; Nie and Sobel 2015; Son et al. 2017; Hendon and Abhik 2018; Martin et al. 2019; among others). Hendon and Abhik (2018) and Abhik et al. (2019) studied the interaction of observed QBO temperature anomalies with the MJO, and proposed that the MJO's unique vertical structure explains why it is especially affected by the QBO. The emergence of the MJO-QBO link in recent decades has also been explored through the lens of MJO-QBO UTLS temperature anomalies (Klotzbach et al. 2019). Yet the specifics of a temperature mechanism have yet to be fully explained or accepted (e.g., Sakaeda et al. 2020).

Here we test the hypothesis that biases in a model's QBO, particularly biases in the UTLS and related QBO temperature variations, can explain why a climate model does not capture a strong MJO-QBO link. We use the CMIP6 version of the

NASA Goddard Institute for Space Studies (NASA GISS) Model E2.1 (Kelley et al. 2020). To minimize QBO biases the model is run in a "nudged" configuration: the zonal-mean zonal and meridional winds in the upper troposphere and throughout the stratosphere in the model are relaxed toward reanalysis, allowing us to study the MJO-QBO connection with minimal QBO biases. Section 2 describes our model, data, methods, and experimental design. Section 3 examines the model QBO and MJO performance, and the MJO-QBO link (or lack thereof). Sections 4 and 5 offer discussion and our conclusions. Additional MJO diagnostics and tests showing that our results are not sensitive to specific parameters or methods related to the nudging, as well as results from an atmosphere-only model simulation, are shown in the appendices.

#### 2. Data, methods, and model

### a. Data and methodology

We make use of several reanalysis and observational datasets. For zonal and meridional winds in analysis and nudging, we use NASA's Modern-Era Retrospective Analysis for Research and Applications 2 (MERRA-2) reanalysis (Gelaro et al. 2017), which has a good representation of the QBO (Coy et al. 2016). To track the observed QBO we use monthly mean MERRA-2 50-hPa zonal-mean zonal wind, averaged from 10°N to 10°S (U50). As in previous studies (Yoo and Son 2016; Son et al. 2017), we define QBOW/E as months when the index exceeds  $\pm 0.5$  standard deviations, respectively. We use the same method to track the model QBO using the model's 50hPa zonal wind. To diagnose the vertical structure of the MJO in observations we use ERA5 daily data (Hersbach et al. 2020) to facilitate comparison to existing literature (e.g., Hendon and Abhik 2018). For observed outgoing longwave radiation (OLR) we use NOAA daily satellite data (Liebmann and Smith 1996). For observed sea surface temperature (SST) we use the Hadley Centre Sea Ice and Sea Surface Temperature dataset (HadISST) dataset (Rayner et al. 2003).

We track the MJO primarily using the real-time multivariate MJO index (RMM; Wheeler and Hendon 2004) and the OLR MJO index (OMI; Kiladis et al. 2014). RMM is a standard MJO index formed using a pair of empirical orthogonal functions (EOFs) of OLR and zonal wind at 850 and 200 hPa. These circulation and convective fields are averaged over the tropics, and the seasonal cycle and mean of the previous 120 days are removed, but no bandpass filtering is done during processing. Projecting daily OLR and zonal wind data onto these EOFs forms two principal component time series, RMM1 and RMM2, that track the strength and location of the MJO. Their phase angle represents the MJO's location, and the amplitude  $(\sqrt{RMM1^2 + RMM2^2})$  represents the MJO's strength. We use the observed RMM index available from the Australian Bureau of Meteorology. For the model RMM index the methodology is identical to that used in observations, except that we project processed model OLR and wind onto the observed EOFs.

Similar to RMM, OMI is a two-dimensional phase space representation of the MJO formed using EOFs. Yet OMI uses subseasonal bandpass-filtered OLR (without any circulation fields). The OMI EOFs themselves are a function of latitude and longitude, as well as day of the year. As a result, the OMI index is smoother and tracks convection more directly than RMM (Kiladis et al. 2014; Wang et al. 2018). We calculate OMI in observations and in the model following Kiladis et al. (2014), but as with RMM we use observed EOFs to project the bandpass-filtered model data. For the phase of OMI, following Kiladis et al. (2014) we reverse the sign of OMI1 and then flip the order of the principal components so that the phases of OMI and RMM approximately align.

We examine the MJO-QBO relationship in December-February (DJF) through three metrics:

- 1) MJO amplitude changes: The MJO is divided into the same eight phases as in Wheeler and Hendon (2004); no amplitude threshold is used, so that even weak MJO days are assigned a phase. We calculate the difference in MJO amplitude (using either RMM or OMI) in each phase between QBOE and QBOW months. We test the statistical significance using a "block" bootstrapping method similar to Henderson et al. (2016) and Henderson and Maloney (2018). This method is similar to a traditional bootstrapping in that it involves random resampling, but rather than sampling individual days at random, blocks of l consecutive days are sampled to account for the autocorrelated nature of the MJO (where l, the length of a block, is a parameter taken from the data). Explicitly, we first calculated, both for QBOE and QBOW winters, the average number of consecutive days the MJO was in a given phase, rounded to the nearest integer and denoted  $l_{OE,OW}$ . This was done separately for each model ensemble member and for observations; values of  $l_{QE,QW}$  ranged from 3 to 5 days per phase for RMM [values consistent in general with Henderson and Maloney (2018)] and from 4 to 8 days per phase for OMI. Next, we let  $N_{OE}$  and  $N_{OW}$  be the total number of days the MJO is in a particular phase in QBOE and QBOW, respectively. From the group of all MJO days in that phase, irrespective of the QBO, we randomly select a series of start dates of size  $N_{\mathrm{QE}}/l_{\mathrm{QE}}$  and  $N_{\mathrm{QW}}/l_{\mathrm{QW}}$  (i.e., the total number of blocks; rounded down) and then select the blocks of  $l_{\rm QE,OW}$  days following these start dates. Finally, we calculate the MJO amplitude difference between those two random groups, repeating this process 5000 times to build up a distribution. Significance here and throughout this study is defined at the 95% confidence level, meaning that the actual differences exceed those in at least 95% of the randomized population (i.e., are less than the 2.5th percentile or greater than the 97.5th percentile).
- 2) *MJO-QBO correlation*: We calculate the DJF-mean RMM/OMI amplitude and DJF mean of a QBO index (we present results exclusively using U50 in DJF, although confirmed that our results hold when defining the QBO at 70, 30, and 10 hPa and in all seasons). We then calculate the correlation over all years; significance is measured with a *t* test, though bootstrapping was also explored (see section 3c).
- 3) MJO activity: We first calculate "MJO-filtered" OLR [similar to the procedure in Wheeler and Kiladis (1999),

Yoo and Son (2016), Son et al. (2017), and Hyemi Kim et al. (2020)] by applying a 20–100-day bandpass filter using a Kaiser window and Python's filtfilt operation to ensure zero phase shift (see Wang 2020). We further filter the data to retain the eastward propagating wavenumber 1-5 signals. We then calculate the standard deviation of the MJOfiltered OLR at each latitude/longitude point to measure MJO activity. To measure the influence of the QBO, we calculate the difference in MJO activity between QBOE and QBOW months. Following Hyemi Kim et al. (2020), for compactness we also calculate the mean of this difference over the warm pool (50°-170°E, 20°S-5°N), a region where both the observed overall MJO activity in DJF and the QBO impact on the observed MJO are highest (Yoo and Son 2016; Son et al. 2017; Hyemi Kim et al. 2020). We assess significance using resampling; here we let  $N_{OE}$  and  $N_{OW}$  be, respectively, the number of QBOE and QBOW months and randomly sample  $N_{\rm OE}$  and  $N_{\rm OW}$  months with replacement from all winter months. We then calculate change in the standard deviation of MJO-filtered OLR between these random samples, repeating this 5000 times. We assess whether the QBOE-QBOW difference exceeds 95% confidence at each grid point.

#### b. Model configurations

We use a CMIP6 version of the NASA GISS GCM for this study: Model E2.1 (Kelley et al. 2020). Model E2.1 has 40 vertical levels, with 15 above 100 hPa, a 2° × 2.5° horizontal resolution, and a model top at 0.1 hPa. We utilize primarily a coupled configuration in which the atmosphere model is coupled to the GISS Ocean model v1 (GO1; in the CMIP6 notation, version E2.1-G, or in CMIP5 notation version E2-R). Versions of E2.1 coupled to the HYCOM ocean model (E2.1-H) also exist and have been submitted to CMIP6, but for brevity we do not consider these [see Schmidt et al. (2014) for a discussion of the two ocean models]. We further explored an atmosphere-only configuration with prescribed SST and sea ice fraction (herein "AMIP"; Rayner et al. 2003), as discussed in appendix B. Compared to the CMIP5 version of Model E (E2; Schmidt et al. 2014), the coupled version of E2.1 has notable improvements (see Kelley et al. 2020). These include improved MJO strength and propagation (Kelley et al. 2020; Rind et al. 2020) achieved via modifications to the cumulus parameterization [following Kim et al. (2012)].

Model integrations are performed from 1 January 1980 through 30 November 2017, with the exception of the unnudged control run (see below), which was initialized on 1 January 1981. The processing of the RMM indices involves removal of a 120-day running mean, so all analysis involving RMM is conducted beginning on 1 May 1980/81. The observational data are always used such that the length of the record in the model and observations is the same.

In the coupled model, the ocean is not initialized from observations, but from a randomly chosen year from a historical run of the coupled model. By choosing different initial ocean states spaced 10–20 years apart, we perform an ensemble of model simulations. Note this means different ensemble

members' initial ocean states can be quite different from one another (e.g., due to ENSO; see section 3c). Here we consider a total of 11 ensemble members (for the control run and sensitivity tests, only one member was used per test).

#### c. Nudging experimental design

A novel aspect of this work compared to previous GCM studies of the MJO-QBO connection is the use of nudging in the stratosphere to attempt to minimize QBO biases. Nudging is also necessary because Model E2.1 does not have a QBO as it is usually run, due to its low vertical resolution and the lack of the necessary adjustments to the gravity wave drag scheme. Nudging (sometimes also called "specified dynamics") is not a new technique (e.g., Ferranti et al. 1990; Jeuken et al. 1996), and nudging in the GISS Model E framework has been developed and utilized in previous studies (e.g., Bauer et al. 2013; Shindell et al. 2013). In principle, nudging should interfere minimally with aspects of the model dynamics other than those with which it is intended to interfere. In this study we nudge the model's zonal-mean zonal and meridional winds in the upper troposphere and stratosphere toward MERRA-2 assimilated reanalysis values. The nudging is carried out by adding a tendency term at each model time step to the zonal and meridional wind, calculated as the difference between the model and the observations. This tendency  $[(\partial x/\partial t)_{\text{nudge}}]$  is calculated as

$$\frac{\partial x}{\partial t_{\text{nudge}}} = \frac{x_{\text{obs}} - x_{\text{mod}}}{\tau},\tag{1}$$

where x is a generic variable (here zonal and meridional wind),  $x_{\rm obs,mod}$  is the reanalysis or model value respectively, and  $\tau$  is a nudging relaxation time scale. For shorter relaxation time scales the model remains closer to the observations: in most results here  $\tau$  is 12 h at all longitudes and latitudes (sensitivity tests with  $\tau=30\,{\rm min},\,1$  week, and 1 month are discussed in appendix B).

As our goal is to test whether the model has an emergent MJO–QBO link, we only nudge the upper troposphere and stratosphere where MJO signals are weak. This is done by only implementing the nudging above a specified model pressure level. To ease the transition from no nudging to nudging, we vary the nudging time scale linearly with height through a transition region. Our transition region is 150–100 hPa, with full nudging above 100 hPa and no nudging below 150 hPa [appendix B considers lower (150–200 hPa) and higher (100–50 hPa) transition regions].

We explored two different implementations of the nudging. In the results shown here we used only "zonal-mean" nudging, which keeps the model close to observations in the zonal mean while allowing zonal variations to evolve freely. The only change in Eq. (1) is that the model and observed zonal means are calculated at each time step before the nudging is applied. If we denote the zonal mean as  $\bar{x}$ , then the numerator on the right-hand side of Eq. (1) becomes  $\bar{x}_{\text{obs}} - \bar{x}_{\text{mod}}$ . In the zonal-mean nudging, the nudging tendency added at a given pressure level, latitude, and time step is the same at each longitudinal grid cell. We emphasize that "zonal-mean nudging" here does *not* mean that the model at each longitude point is nudged

toward the observed zonal mean [as would be the case if the right-hand side of Eq. (1) were  $\overline{x}_{\rm obs} - x_{\rm mod}$ ]. Rather, our methodology constrains the model only in the zonal mean, allowing zonal asymmetries to exist and for the model's zonal structure to differ from reanalysis. An alternative strategy, which we call "grid-point" nudging, relaxes the full 3D structure of the model at each latitude, longitude, and relevant pressure level to reanalysis. Results from grid-point nudging are presented in the appendices.

The advantage of the zonal-mean nudging is that the zonal structures of any vertically propagating waves from the troposphere into the stratosphere are not damped by nudging. The advantage of the grid-point nudging is that the model retains the zonal structure of the reanalysis. Since the QBO is fairly zonally symmetric, this impact may not be of central importance, although Densmore et al. (2019) discussed a possible link between the MJO–QBO relationship and zonal asymmetries in QBO temperature anomalies and Tegtmeier et al. (2020) have more recently highlighted the zonal asymmetries of QBO temperature signals. We prioritize the zonal-mean nudging as preliminary tests showed more promising results in that configuration, but found our results are not sensitive to grid-point vs zonal-mean nudging (see the appendices).

Finally, in most runs we nudge to MERRA-2 assimilated reanalysis fields, and in all ensemble members we nudge the stratosphere identically. However, to explore whether increasing or decreasing the magnitude of the QBO has an effect on our results, in the appendices we carried out sensitivity tests multiplying the meridional and zonal wind by a factor of 1.5 or 0.5 to look at whether stronger or weaker stratospheric winds have a noticeable impact on the MJO. Table 1 lists the experiments in this study, including our sensitivity tests.

# 3. Results

## a. QBO performance

We first examine the model representation of the QBO both in a control simulation without nudging and in the nudged model. Figure 1 shows the 10°N–10°S and zonally averaged zonal winds in MERRA-2, the control run, and the model with nudging. Also shown is the difference between the nudged model and observations. In observations, descending easterly and westerly wind regimes in the stratosphere are very clear, whereas in the control version of the model there is no QBO: the stratospheric wind is weakly easterly with little variation.

With nudging, the QBO is very well represented compared to reanalysis. By eye, it is clear the nudged model overall captures the observed amplitude, period, and descent rate of the QBO. The correlation between the model and observational QBO winds in Fig. 1 at 100, 70, 50, and 30 hPa is above 0.98. The mean difference in the wind between the observations and model is on the order of 0.2–0.3 m s $^{-1}$  between 100 and 30 hPa. Slightly higher differences exist at 30 hPa (around  $2.2\,\mathrm{m\,s^{-1}}$ ), but this bias still represents a small difference (e.g., Fig. 1d) given that QBO anomalies in general at that level can be on the order of  $10{\text -}30\,\mathrm{m\,s^{-1}}$  in amplitude.

TABLE 1. List of experiments in this study per the configurations and nudging parameters described in section 2. The columns describe, respectively, whether the model ocean state is specified ("AMIP") or coupled; whether the grid-point or zonal-mean nudging is used (see section 2c); the nudging time scale [ $\tau$  in Eq. (1)]; the nudging transition region (no nudging below the region, and full nudging at  $\tau$  above the region); the strength of the QBO; and the size of the ensemble. Runs beneath the blank row are the sensitivity tests discussed in appendix B. Obs. = observed.

Model version	Nudging style	Nudging time scale $(\tau)$	Nudging transition height	QBO strength	Ens. size
E2.1 Coupled	None	_	_	None	1
E2.1 Coupled	Zonal-mean	12 h	150–100 hPa	Obs. QBO	11
E2.1 AMIP	Zonal-mean	12 h	150-100 hPa	Obs. QBO	1
E2.1 Coupled	Grid-point	12 h	150–100 hPa	Obs. QBO	1
E2.1 Coupled	Zonal-mean	30 min	150–100 hPa	Obs. QBO	1
E2.1 Coupled	Zonal-mean	1 week	150–100 hPa	Obs. QBO	1
E2.1 Coupled	Zonal-mean	1 month	150–100 hPa	Obs. QBO	1
E2.1 Coupled	Zonal-mean	12 h	200–150 hPa	Obs. QBO	1
E2.1 Coupled	Zonal-mean	12 h	100–50 hPa	Obs. QBO	1
E2.1 Coupled	Zonal-mean	12 h	150–100 hPa	$1.5 \times \text{Obs. QBO}$	1
E2.1 Coupled	Zonal-mean	12 h	150–100 hPa	$0.5 \times \text{Obs. QBO}$	1

Below the nudging levels (100 hPa), the control and nudged versions of the coupled model also show differences (Fig. 1). Climatologically, the nudged model has winds more closely resembling observations than the coupled control, even at lower levels where nudging is not implemented. The nudged model tends to have weaker westerlies in the upper troposphere and a less pronounced annual cycle than the control simulation, displaying reduced tropospheric wind variability. The cause of this reduction is not known, and while it may be

examined more in future work it is not investigated here. Still, it is noteworthy as it suggests the stratosphere in this model has at least some impacts in the troposphere when nudging is imposed.

Model temperatures are not nudged, but nudging the wind (combined with thermal wind balance) leads to realistic QBO temperature anomalies. Figure 2 shows the QBOE minus QBOW temperature differences for the nudged model and observations. The model reasonably represents both the strength and structure

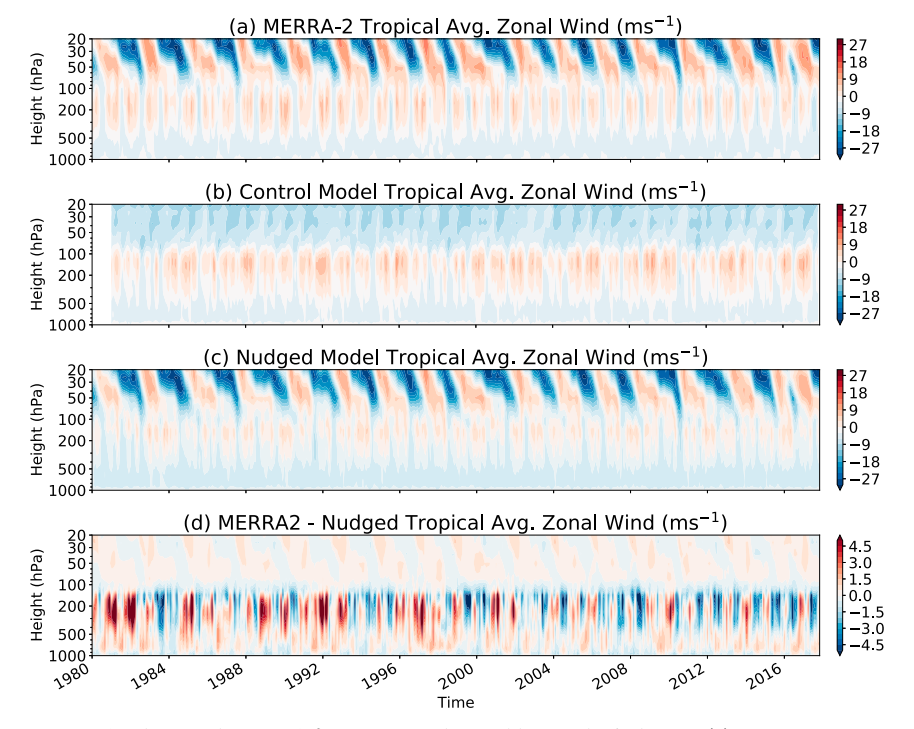


FIG. 1. The zonal-mean, 10°N/S averaged monthly zonal wind from (a) MERRA-2 reanalysis, (b) the coupled model without nudging, (c) the coupled model with nudging, and (d) reanalysis minus the nudged model.

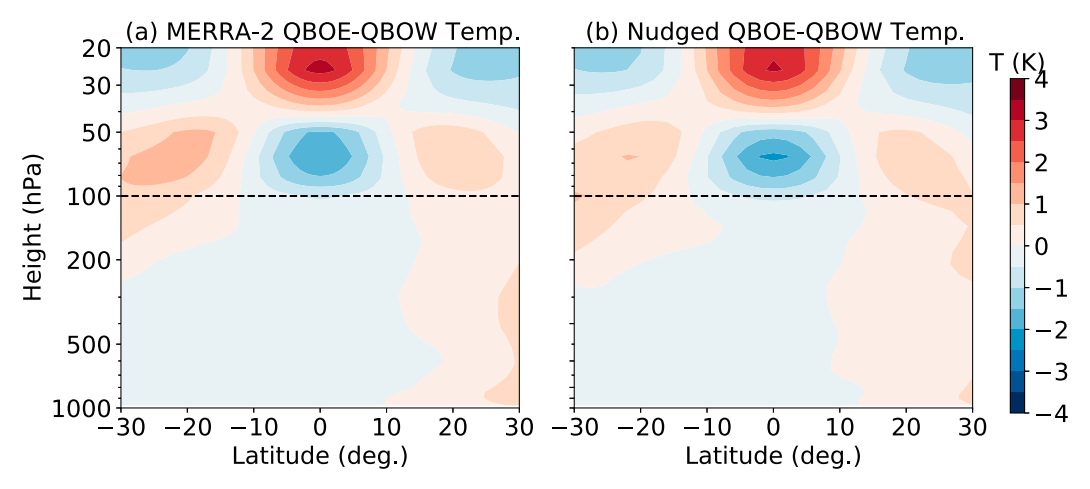


FIG. 2. Zonal-mean QBOE minus QBOW temperature anomalies as a function of latitude and height in (a) MERRA-2 and (b) the coupled nudged model. The horizontal dashed line is at 100 hPa, above which full nudging is applied. The observations have been interpolated onto the model grid to facilitate comparison.

of the observed temperature anomalies, especially in the UTLS. The off-equatorial warm anomalies are also captured in the UTLS (Baldwin et al. 2001), although they are slightly weaker in the southern extratropics in the model compared to observations for unknown reasons. Overall, this demonstrates clear improvement to QBO-associated temperature signals in the UTLS relative to other CMIP6 models that simulate internal QBOs, where typically models' QBOE–QBOW temperature differences are often on the order of half what is observed (e.g., Hyemi Kim et al. 2020).

Figure 3 shows times series of U50 zonal wind and 100-hPa temperature (processed the same way as U50), where the shading represents the range across ensemble members. The top panel confirms that U50 is essentially identical both between the model and observations, and between different model ensemble members (shading is plotted, but differences are too small to be visible). This is by construction due to the short nudging time scale.

Model temperature anomalies at 100 hPa show more variability across the ensemble members, as well as between the model and observations. The nudged model matches the observed variability better than the control matches observations, although both the nudged and control versions are biased warm: the control run is approximately 2.5 K too warm, while the nudged model is approximately 1.5 K too warm, with more bias in the easterly phase of the QBO compared to the westerly phase. The nudged model temperature bias at 100 hPa also shows a strong seasonality: the model is around 1.9 K too warm in December-February, with only a bias of 0.25 K in June-August. Differences in temperature are likely due to the fact that the temperature is not nudged. Further, the winds below 100 hPa are nudged less stringently, leading to more variability in the vertical structure of the zonal wind around 100 hPa. Via thermal wind, this is consistent with more variability in the temperature signals. Finally, it is also the case that tropospheric convection and/or upwelling waves can affect temperatures at 100 hPa, including convection associated with the MJO (as addressed in section 3b). Differences between those processes in different ensemble members may further contribute to variability in this region.

Overall, the model with nudging captures the QBO with high fidelity in zonal wind, and shows realistic temperature variability associated with the QBO. The change in the stratospheric winds is stark compared to the control run, which lacks a QBO, and appears to have some impact on the troposphere, as evident by changes in the winds below 100 hPa in Fig. 1. The model is still biased somewhat warm at 100 hPa, especially during winter, and the magnitude of the warm bias (~1.5–2 K) is comparable to the overall amplitude of QBO temperature changes there. But in general the model simulates the variability of QBO temperature signals better than most models with a free-running QBO. We now turn to the model's representation of the MJO.

# b. MJO performance

While nudging acts to minimize QBO biases, the MJO biases in the model are more difficult to control for given that the model MJO should be allowed to freely respond to stratospheric changes. In general, we find that the MJO is well represented in Model E2.1 for a GCM of this resolution (see also Kelley et al. 2020). Still, we diagnose several potentially important model biases that may have a bearing on the MJO-QBO connection. We focus in this section on the MJO as represented in the nudged model, since the control simulation's MJO performance is comparable to the nudged simulation (not shown in detail). In addition, we ensured that our nudging procedure does not impact the MJO in such a way as to bring the nudged model MJO toward the observed MJO; analysis for example of the correlation between each ensemble member's RMM and OMI index versus observations showed no correlation in any instance. Additional MJO diagnostics are presented in appendix A.

Figure 4 shows a general comparison of DJF-mean OLR and MJO-filtered OLR in the nudged model and observations.

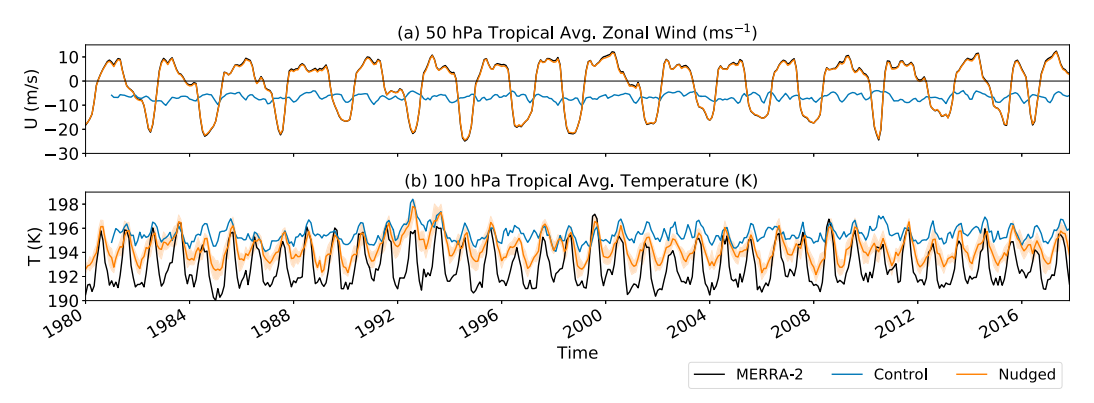


FIG. 3. (a) The U50 QBO index (section 2a) for observations (black), the control simulation (blue), and the nudged model (orange). (b) The temperature at 100 hPa, processed identically to the U50 index. Shading shows the minimum and maximum at each month across all ensemble members. For U50 shading is plotted, but variations are essentially zero, and the model and observed curves largely overlap.

Here all 11 ensemble members are averaged together, as individual ensemble members are comparable to the ensemble mean (not shown). MJO-filtered OLR here is defined as in section 2a as 20–100-day and eastward wavenumber 1–5 filtered OLR.

Comparing the observed and model DJF-mean OLR, we find the model simulates the same overall regions of strong convection (low OLR) during DJF as observed: equatorial Africa, the warm pool, and the Amazon show minima on and south of the equator. Overall the model has comparable values to observed in these regions, although the model is biased slightly high, indicating convection is somewhat too shallow.

Also notably, the model's strong convection extends too far to the east into the central Pacific, and the OLR minimum there lies too far north, as evident by the large negative anomaly in the difference plot centered around 130°W (Fig. 4e). Another salient feature of DJF-mean convection is that the model tends to have too weak convection in the Northern Hemisphere extratropical Pacific.

Convection associated with the MJO shows similar overall patterns: the model captures the peak in MJO activity with a maximum just south of the equator over the Maritime Continent. However, MJO convection, like mean convection, is too active in the east Pacific. We hypothesize this may be due

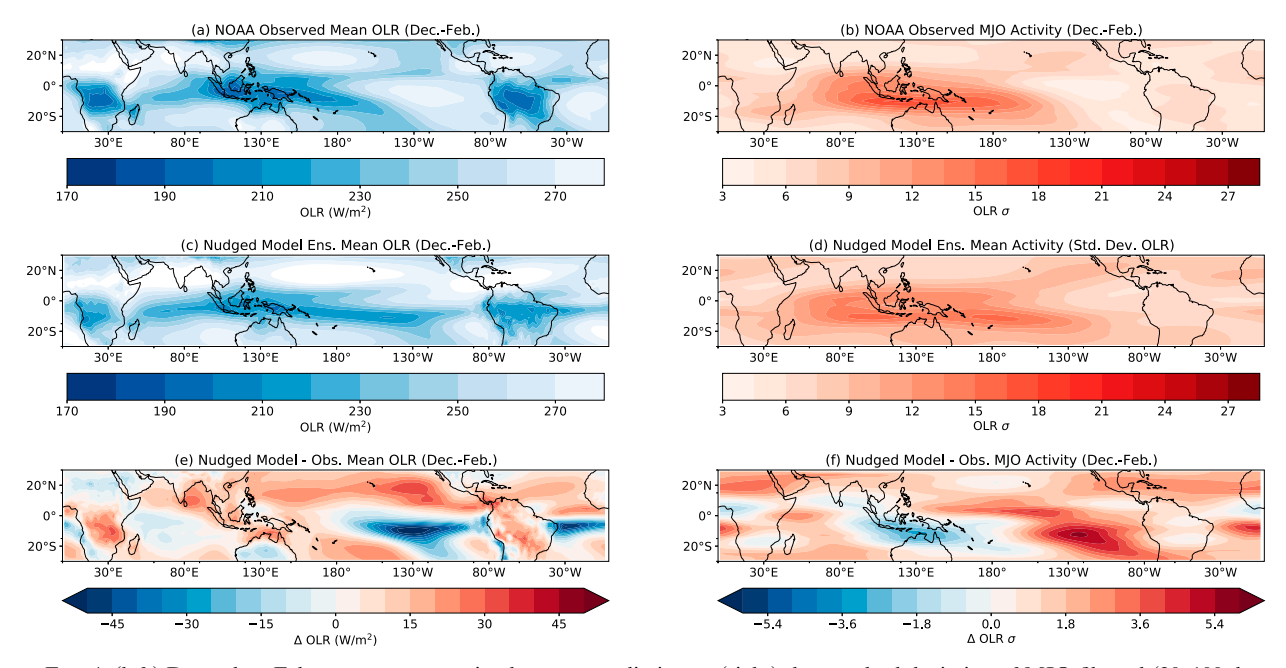


FIG. 4. (left) December–February mean outgoing longwave radiation or (right) the standard deviation of MJO-filtered (20–100 day, eastward wavenumber 1–5) outgoing longwave radiation. (a),(b) Observations, (c),(d) the ensemble mean of the nudged model, and (e),(f) model minus observations.

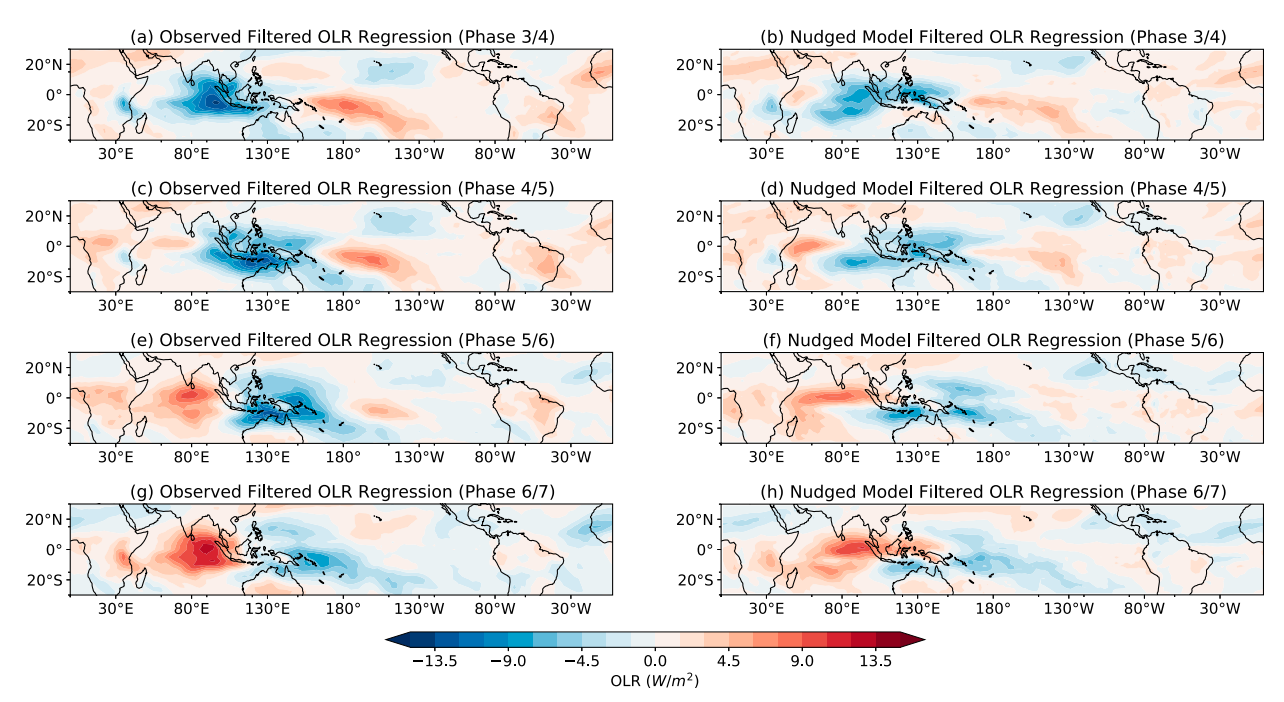


Fig. 5. (a)–(h) Regression plots of 20–100-day filtered outgoing longwave radiation, regressed against RMM1 – RMM2, RMM1, RMM1 + RMM2, and RMM2, corresponding to MJO phases 3/4, 4/5, 5/6, and 6/7 (each row). The regression coefficient is multiplied by the standard deviation of OLR. (left) Observations, and (right) the model.

to ENSO, which is too strong in this model (see Kelley et al. 2020), or some other process that allows the MJO to extend into the east Pacific [as discussed, e.g., in Son et al. (2017)]. Of particular potential significance to the MJO–QBO link, model MJO activity also shows a relative decrease around the Maritime Continent compared to observations (see Fig. 4f around 130°E). As this is both the region of maximum MJO activity in observations as well the region that appears most influenced by the QBO in observations (Son et al. 2017; Densmore et al. 2019; Zhang and Zhang 2018; Fig. 9), weakerthan-observed MJO activity here could be important for the MJO–QBO relationship in this model if MJO convection is not deep enough, MJO activity is too low, or MJO convection in this region is poorly simulated.

To further examine the vertical and horizontal structure of the MJO, following Virts and Wallace (2014) and Hendon and Abhik (2018) MJO-related variables are regressed against an MJO index (here we use RMM). In this analysis, a single ensemble member is used to facilitate comparison to observations. Figure 5 shows OLR pattern formed by regressing 20–100-day bandpass-filtered DJF OLR onto RMM1 – RMM2, RMM1, RMM1 + RMM2, and RMM2, which roughly correspond to MJO phases 3/4, 4/5, 5/6, and 6/7, respectively. Regression coefficients are scaled by the standard deviation at each grid point to recover physical units, and the resulting patterns represent linear differences between symmetric MJO phases (e.g., between phases 3/4 and 7/8, 4/5 and 8/1, etc.).

The eastward propagation of MJO signals, starting with strong negative OLR anomalies west of the Maritime Continent and ending with positive anomalies in the same region, is evident in both the model and observations. However, note that the model displays lower amplitudes in the active and suppressed MJO phases than observed, for example around 90°E in the phase 3/4, or around the Maritime Continent (130°E) in phases 4/5 and 5/6. Model MJO signals in particular are both too weak around the Maritime Continent, and show different spatial structure (consistent with Fig. 4): the observed peak of MJO convective activity in phases 4/5 and 5/6 tends to be a fairly compact center of activity just south of the Maritime Continent and north of Australia, whereas model signals are more dispersed spatially, weaker in magnitude, and in particular in phases 4/5 peak too far west. Suppressed MJO conditions also tend to be weaker in the model than observed (e.g., around the date line in phases 3/4 and 4/5) and in MJO phases 5/6 and 6/7 the model suppressed phase is weaker and less evident south of the equator. These biases in MJO convective strength, structure, and location may be important to any possible MJO-QBO link in this model.

Hendon and Abhik (2018) argued that the MJO's vertical structure might also have importance for the MJO-QBO link. The strong, vertically stacked nature of MJO convection, and the fact that MJO deep convection is associated with "cold cap" temperature anomalies above regions of enhanced convection (Holloway and Neelin 2007) are highlighted in their work. Figure 6 examines the vertical structure of the MJO in DJF in observations versus the coupled model (one ensemble member was used). This plot was made following Hendon and Abhik (2018), and readers are referred to that study for the full methodology. In brief, shown in Fig. 6 are longitude-height regressions of MJO temperature, zonal wind, and vertical

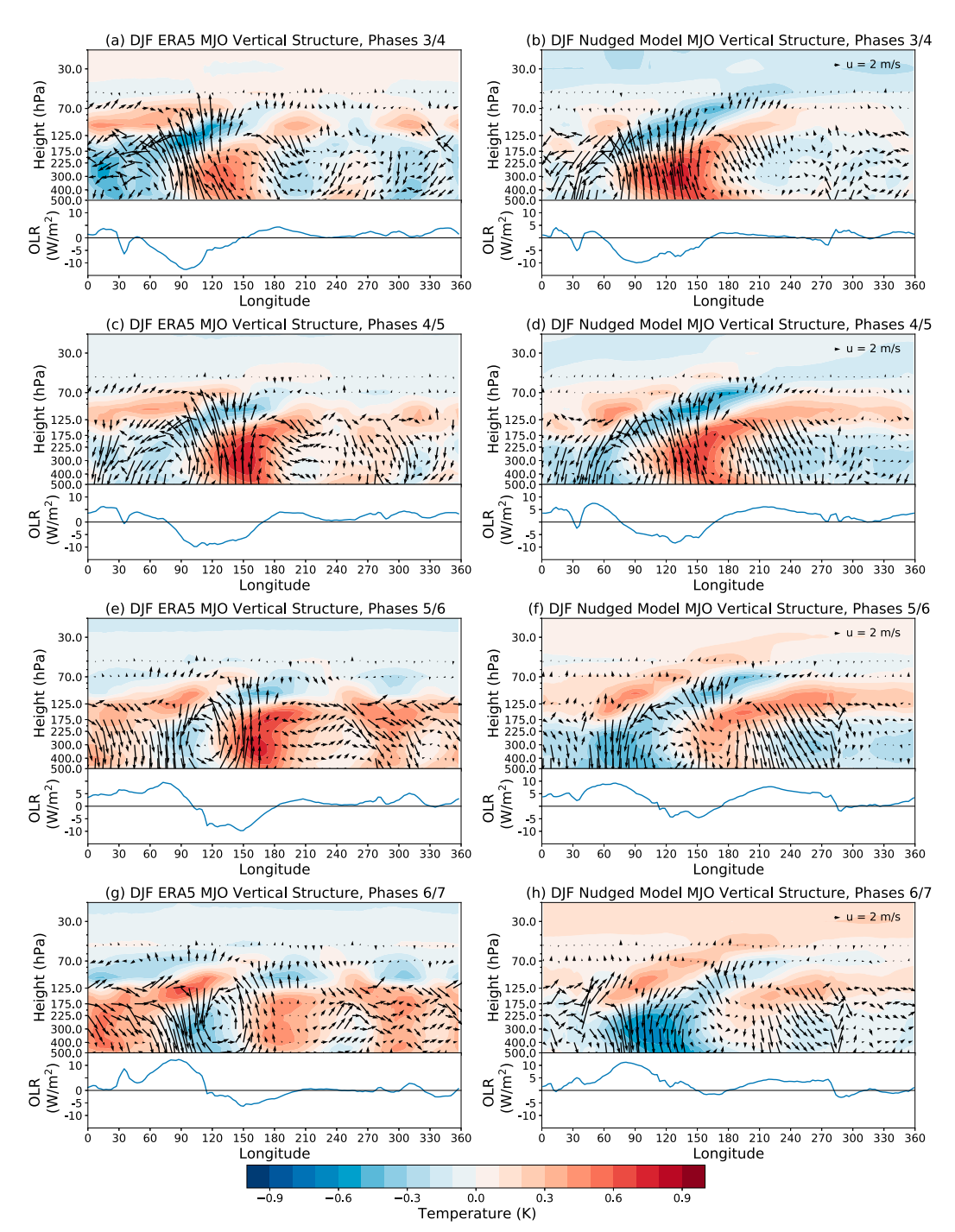


FIG. 6. Longitude–height regression plots of DJF MJO temperature, zonal wind, and vertical velocity as well as OLR (bottom portion of each panel) similar to Fig. 5. Variables are averaged from 5°S to 5°N, and the seasonal cycle is removed before regressing against RMM1 - RMM2, RMM1, RMM1 + RMM2, and RMM2. The regression coefficient is multiplied by the standard deviation of each variable. Vertical velocity is multiplied by -1 (upward indicates ascent), and by 1000 for ease of interpretation. The y axis is log pressure.

velocity similar to those in Fig. 5, except that no bandpass filtering is used to facilitate comparison to Hendon and Abhik (2018). Regressions are formed by averaging variables over 5°N/S and removing the seasonal cycle. The resulting plots

show the MJO vertical structure in the upper troposphere and lower stratosphere as it propagates from the Maritime Continent into the west Pacific. The bottom of each panel shows regressed OLR.

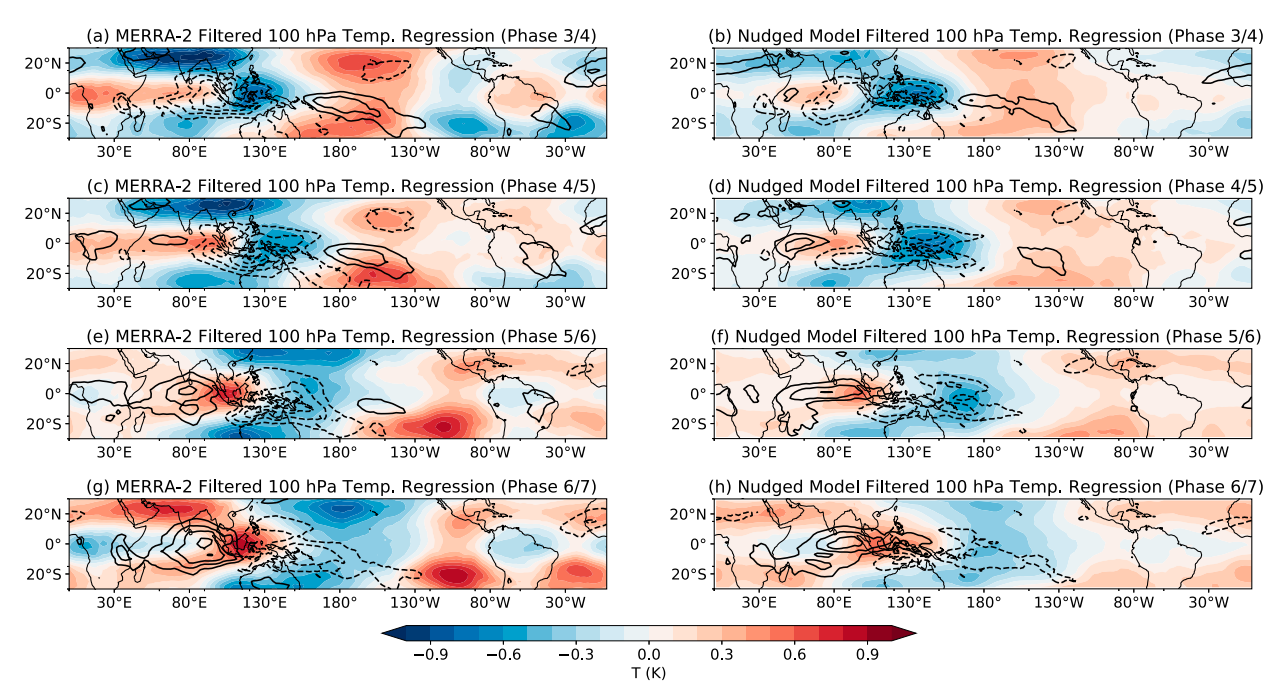


FIG. 7. As in Fig. 5, but for 100-hPa bandpass-filtered temperature (shading). Contours are OLR from Fig. 5, with contours from -12 to 12 W m<sup>-2</sup> in 3 W m<sup>-2</sup> intervals; the zero contour is omitted, and negative contours are dashed.

In Fig. 6 we do not segregate by QBO phase, since we are interested in this section in whether the model gets the overall MJO structure correct. In general, the OLR and the vertical structure of the MJO are consistent between the model and observations, but potentially important model biases are still evident. In phase 3/4, negative OLR anomalies associated with enhanced convection around 90°–120°E are flanked on either side by suppressed convection, and subsequently propagate east. The model shows weaker negative OLR anomalies than observed, especially from phases 4/5 to 6/7, consistent with Fig. 5.

In terms of the vertical structure, in phase 3/4 the model has weaker vertical ascent in the active phase, especially in the uppermost part of the troposphere. A cold cap is evident in the model and observations around 120°-150°E, which extends farther into the UTLS in the model than observed. The model also does not show the significant cold tropospheric and warm stratospheric anomalies around 30°-60°E during phase 3/4 that observations show. As the MJO propagates east, model biases become more evident, and the model shows much weaker temperature and vertical velocity anomalies in the upper troposphere compared to observations (see, e.g., phase 5/6 around 150°-180°E and phase 6/7 around the date line). Coupled with the weaker OLR, this suggests that MJO convection in the model does not penetrate as high into the troposphere as vigorously as in observations. Model MJO signals in the UTLS temperature also show more tilt upward and to the east than observations. Thus it appears that the MJO convection is less coherent in the model and perhaps more Kelvin wave-like than in observations [see Abhik et al. (2019) for a comparison of MJO and Kelvin wave vertical structures in observations].

Finally, Fig. 7 shows a regression plot similar to that in Fig. 5, but for the 100-hPa temperature in shading; OLR anomalies from Fig. 5 are repeated here in contours. As both MJO and QBO modulation of TTL temperatures have been hypothesized to play a role in the MJO-QBO link, it is important to understand the degree to which the model MJO reproduces observed temperature signals around the tropopause. Recall that, because nudging is only applied in the zonal mean and temperature is not nudged, the zonal structure of temperature at 100 hPa is not tightly constrained by the nudging and is more free to evolve in the model. Figure 7 shows that the overall features of MJO temperature signals in the UTLS and their relation to convection are captured by the model. The model captures cold anomalies at 100 hPa on the equator associated with the "cold cap" discussed above (e.g., anomalies around 130°E in phase 3/4 that subsequently move east), which generally sit to the east of the strongest convection. The amplitude of this equatorial cold anomaly is comparable in the model to that in observations across most phases. However, the corresponding warm anomaly to the west is weaker in the model than observed, especially around phases 5/6 and 6/7, and has a shorter longitudinal extent in the model than observations.

While the on-equatorial temperature anomalies are similar in the model and observations, off the equator in the subtropics the model tends to show weaker-than-observed temperature signals. This is especially evident around 20°N, where in most phases the observations show stronger temperature signals than the model. As noted, for example in Virts and Wallace (2014), the overall structure of the temperature signal in the

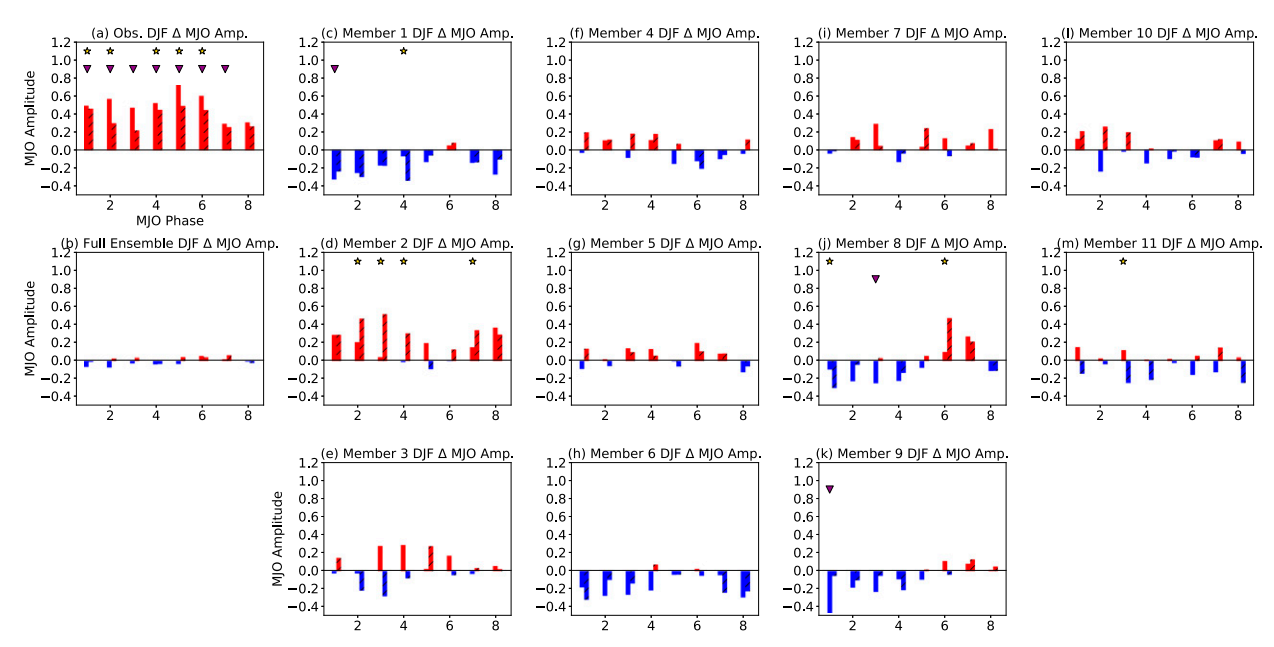


FIG. 8. QBOE minus QBOW changes in the amplitude of OMI (left bars) and RMM (right bars, hatched) as a function of MJO phase. Red and blue bars indicate positive or negative differences. (a) Observations, (b) all ensemble members, and (c)—(m) individual ensemble runs. Gold stars at the top indicate the differences for RMM are significant via a block bootstrapping test (section 2), and purple arrows indicate OMI changes are significant.

model and observations seems consistent over the warm pool with an idealized "Gill-type" response to a heat source on the equator (Matsuno 1966; Gill 1980), and these off-equatorial signals are thus suggestive of a Rossby wave response, which (at least in temperature) seems too weak in the model. However, it is unclear whether off-equatorial temperature anomalies have any bearing on the MJO-QBO link in observations.

Overall, Figs. 5–7 suggest that while the horizontal and vertical structure of the model MJO is similar to observations, there are still biases that may play an important role in the MJO–QBO link. Convection is generally too weak and less active around the Maritime Continent in the model versus observations, and the vertical structure tends to show lower than observed vertical velocities in the upper troposphere. While the model is capable of capturing the approximate behavior of the cold cap in near-tropopause temperature which sits above and to the east of convection in most MJO phases, in certain phases these temperature anomalies in the model appear somewhat weaker than observed, as are MJO temperature signals in the extratropics.

Additional general MJO features like the seasonal cycle are assessed via the OMI and the RMM index and are presented in the appendices. In general, both RMM and OMI diagnostics are comparable between the model and observations. Differences are somewhat more pronounced in OMI, and are consistent with weaker and less coherent MJO convection in the model than observations. The model MJO convection viewed through the OMI index also exhibits biases in the seasonal cycle that may be important. These biases in the MJO should be kept in mind in the next section, where we explore

whether the drastic changes made in the stratosphere discussed in section 3a have any impact on the MJO.

## c. MJO-QBO relationship

We first examine the MJO-QBO connection via QBOE minus QBOW differences in the strength of the MJO. Figure 8 shows the QBOE minus QBOW differences in RMM and OMI amplitude as a function of MJO phase. We plot the observations, the response across the full ensemble, and each individual ensemble member. In observations, a strong and consistent modulation of the MJO is evident in all phases in both OMI and RMM, and is statistically significant in most phases as measured with either index, especially in the Indian Ocean and Maritime Continent. The same cannot be said of the model. Combining all ensemble members, no QBOE minus QBOW differences are strong or significant in Fig. 8b.

The full-ensemble signal is also not necessarily representative of individual members, where larger changes are evident. However, QBOE–QBOW differences in individual ensemble members are rarely significant and often not of the correct sign. Instead, the ensemble members show a wide range of apparent MJO–QBO relationships. For example, member 2 shows relatively consistent increases in MJO activity in QBOE relative to QBOW in the OMI index, although no significant change in RMM. However, other members such as members 1 (Fig. 8c) and 6 (Fig. 8h) show MJO signals that are stronger in QBOW, the opposite sign to that observed. In all runs except ensemble member 2, changes are either not significant, or are only significant for a particular index in one or two phases, which seems likely due to chance.

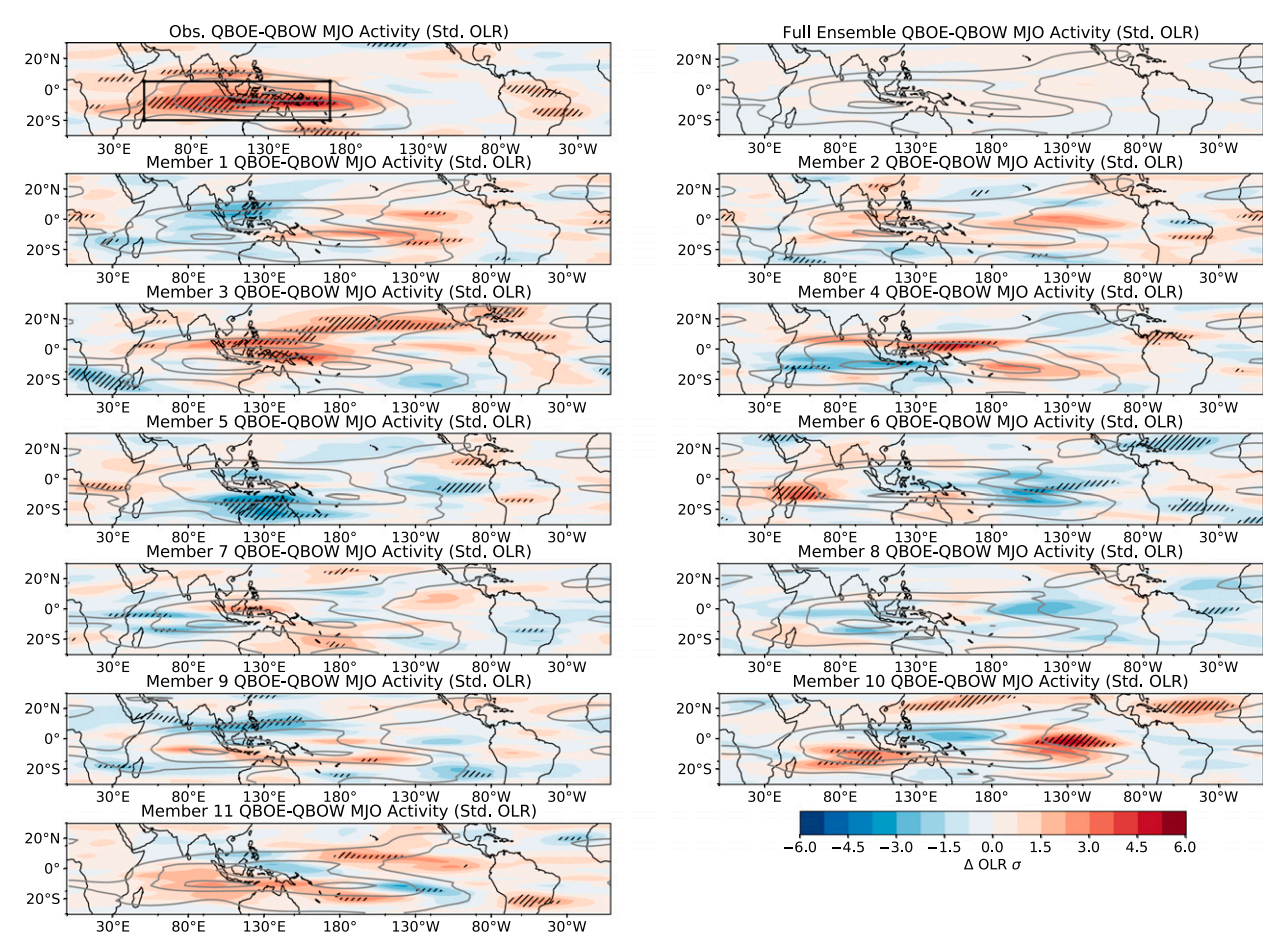


FIG. 9. The QBOE minus QBOW difference (colored shading) in the standard deviation of MJO-filtered OLR, as described in section 2. (top left) Observations, (top right) the full ensemble, and (bottom rows) individual ensemble members. Gray contours show the DJF climatology of the standard deviation of MJO-filtered OLR: contours are from 9 to 24 W m $^{-2}$  at 3 W m $^{-2}$  intervals. Significant differences are hatched. The black box in the top left indicates the warm pool region (50°–170°E, 20°S–5°N).

It is noteworthy, however, that changes that are very small in the ensemble mean are often much larger in individual ensemble members. This suggests that over the span of approximately 40 years, it is possible to get relatively large QBOE–QBOW differences due simply to internal variability. Still, these differences in the model are not significant using a block-bootstrap, whereas in observations strong and significant modulation is more evident. This both suggests that care should be taken in properly formulating statistical tests when the number of years considered is relatively small and recommends the continued use of ensemble model experiments to examine the MJO–QBO link. However, it also seems to indicate relatively clearly that the signal seen in observations is larger than that which could arise due to chance in this model.

Additional analysis of the MJO-QBO connection using other metrics confirms that this model does not have a strong MJO-QBO link, even in particular ensemble members. Figure 9 shows the QBO change in MJO-filtered OLR activity, as well as the DJF climatological MJO activity (contours). The

11 members show similar climatological MJO signals, although as discussed in section 3b MJO activity is too weak around the Maritime Continent. Observations show a clear increase in the MJO activity in QBOE versus QBOW over the warm pool, where the MJO is most active, with statistically significant increases across much of the Indian Ocean and Maritime Continent. In contrast, the full model ensemble shows no strong signal and no significance at any point. Individual members show a range of different responses, but none is as strong as that in observations and only a few ensemble members showing broad regions of significant increase or decrease. Furthermore, those ensemble members (e.g., members 3, 5, and 10) that show significant signals often do so outside the Maritime Continent (e.g., member 10) or have the opposite sign to observation (e.g., member 5). It is also the case that ensemble members that showed a strong MJO amplitude change (e.g., member 2) show less of a clear response in the MJO-filtered OLR standard deviation. This is unlike observations, where a clear MJO-QBO link is evident in all three metrics we used.

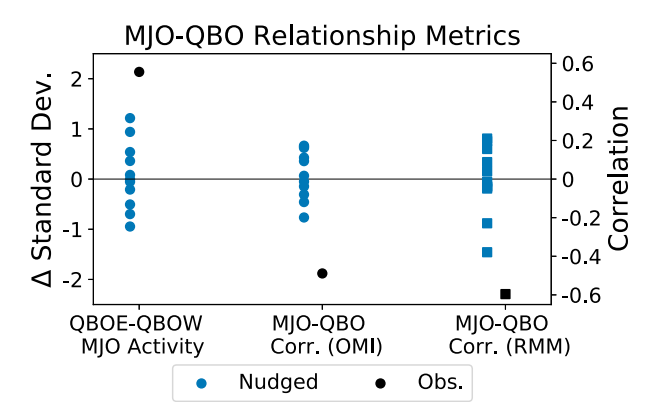


FIG. 10. The warm pool averaged QBOE minus QBOW changes in MJO activity (e.g., Fig. 9) for the 11 coupled ensemble members (blue) and observations (black) is shown on the left. The correlation between DJF-mean OMI (center; circles) or RMM (right; squares) amplitude and U50.

Figure 10 summarizes these findings by showing, in the left column, the change in the standard deviation of MJO-filtered OLR averaged over the warm pool. The ensemble members show a wide spread around zero, far from the observed change of more than two standard deviations. Also shown in Fig. 10 is our final MJO-QBO metric: the correlation between the DJFmean MJO amplitude and the U50 index. The center and right panels show the correlation coefficient between OMI/RMM and U50 for all 11 members. Consideration of the full ensemble together also shows no strong correlation (not shown). Examination at levels other than 50 hPa and in other seasons apart from DJF also showed no strong results (not shown). Only one of the coupled ensemble members, member 2, shows a significant correlation in winter that is comparable to the observed, with a model coefficient of -0.38 compared to the observed coefficient of -0.60. However, member 2 is still weaker than observed, and does not show a strong MJO-QBO correlation in OMI.

We hypothesize the significance of this single ensemble member in a single season using RMM is due to chance. In 11 ensemble members with four seasons, one would naively expect one or two seasons to show significant correlation at the 95% confidence level by chance. To confirm this, we performed a bootstrapping analysis in which we randomly sampled 38 QBO and RMM/OMI values from all seasons across all ensemble members and computed the MJO-QBO correlation. We repeated this 5000 times. This analysis confirmed at  $\sim$ 5% of the bootstrapped resampling showed a correlation that was significant at the 95% confidence level. This indicates that spurious correlation or significance in the model does seem possible given a relatively short record and the interannual variability of the MJO. Thus, we believe it is important to emphasize the need to examine the MJO-QBO link in models via several metrics.

Measured across all three of our metrics and using multiple MJO indices, it seems clear both that there is no link in this model, and that the observed MJO-QBO relationship is distinct from the internal variability of the model. These conclusions

are additionally supported by our experiments, described in the appendices, in which various nudging parameters were changed, or in some cases the strength of the QBO itself was artificially increased or decreased. In those experiments as well, in no case is a strong MJO–QBO link seen, suggesting our conclusions are not sensitive to the way in which we implement the nudging.

#### d. Possible missing mechanisms

What explains both the apparent diversity of the MJO–QBO interaction across different ensemble members, and the overall lack of an MJO–QBO link? Because the stratosphere is nudged and is largely identical across the ensemble members, it seems unlikely that stratospheric processes explain the differences across the ensemble members. To explore this question more, we examined two hypotheses: 1) the difference in the sea surface temperature among the coupled model ensemble members may play a role in the ensemble's different MJO–QBO relationships and 2) the model may not properly capture QBO changes to high clouds in the tropics, which have been hypothesized as important for the MJO–QBO connection (e.g., Son et al. 2017; Sakaeda et al. 2020).

First, we examined whether there was any strong connection between particular SST patterns and our MJO-QBO metrics. Note that our nudging framework prevents the model QBO from responding to the SST (or to related changes to convection, gravity wave fluxes, or other atmospheric quantities influenced by SST). Thus, here we explored the specific hypothesis that the MJO-QBO relationships in the coupled model could be influenced by internal SST variability that is independent of the stratosphere (e.g., SST variability that coincidentally aligns in some way with the nudged QBO in some members but not others). The role that SSTs may play in the MJO-QBO link is further explored via the AMIP simulations discussed in the appendices, as that simulation contains the prescribed SST.

Figure 11 shows QBOE minus QBOW SST composites in the observations and the coupled model runs. The observations show a La Niña-like pattern, with the signature cooling in the equatorial eastern Pacific. This apparent QBO-ENSO connection has been noted in other studies (e.g., Garfinkel and Hartmann 2007; Christiansen et al. 2016; Domeisen et al. 2019), and the present thinking is that any observed QBO-ENSO relationship is nonlinear, weak, or coincidental. The observed MJO-QBO link holds in ENSO neutral years (Son et al. 2017; Nishimoto and Yoden 2017), and it seems unlikely that ENSO is relevant to the observed MJO-QBO connection (Sakaeda et al. 2020). Still, it is somewhat surprising that any SST pattern clearly stands out on OBO time scales.

As expected, the model ensemble members show a range of SST states, although in the full ensemble no clear SST pattern is associated with the QBO. We found no clear connection between the MJO–QBO link across ensemble members and any pattern of SST variability, or ENSO behavior. Examination of whether warm pool SST changes in QBOE versus QBOW across ensemble members were linked to changes in MJO activity showed no strong linear correlation (not shown). No strong or significant correlation between the QBO and ENSO

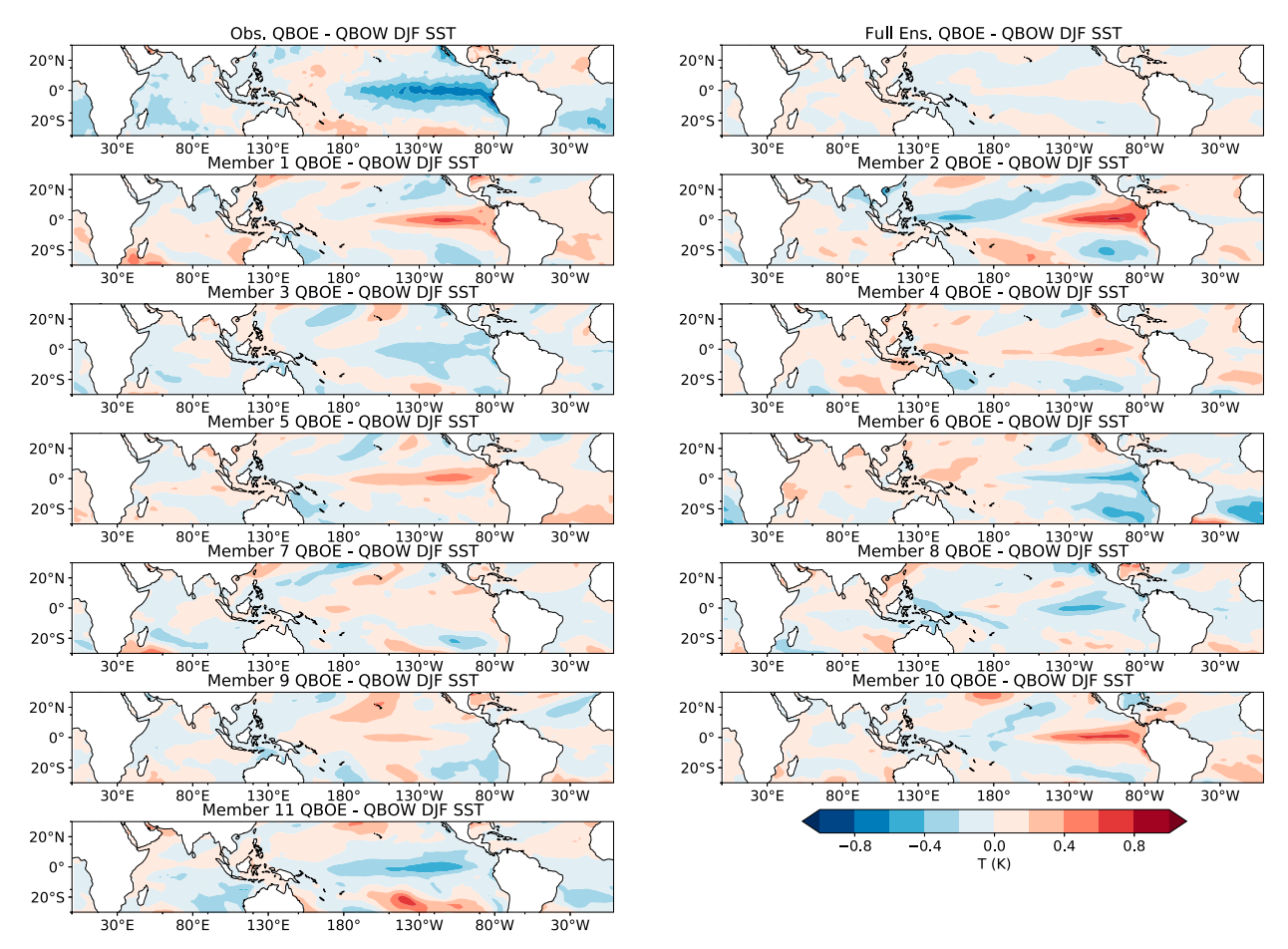


FIG. 11. The QBOE minus QBOW difference in sea surface temperature during December–February for (top left) observations, (top right) the full coupled ensemble, and (bottom rows) individual ensemble members.

(measured using the Niño-3.4 index) was found generally across the model ensemble. The ensemble member with the nearest to observed MJO-QBO link (member 2) shows an SST pattern that looks largely distinct from observations, including a weak El Niño signal in the east Pacific (opposite the observed pattern). This suggests that SST patterns in this model do not exert a strong influence on any apparent MJO-QBO connection or variability across the ensemble.

We further conducted some preliminary analysis of the model's high cloud response to the imposed QBO. Here we examine in particular whether the nudged QBO modulates high clouds in a manner qualitatively consistent with observations, in which increased high cloud cover is observed during QBOE (e.g., Son et al. 2017). The impact of high clouds on the MJO, and the modulation of high clouds by the QBO, has been proposed as a potential pathway that could connect the QBO and MJO in observations (Son et al. 2017; Sakaeda et al. 2020), although detailed studies on any high cloud influence on the MJO–QBO link have not been carried out. Still, were the model to lack this high cloud response to the QBO, it might help explain the lack of a strong MJO–QBO relationship.

In Fig. 12, we plot the QBOE minus QBOW high cloud fraction in the model, as well as the 100-hPa temperature

difference in contours. Here we do not compare to any observed product. Figure 12 demonstrates that, consistent qualitatively with findings in Son et al. (2017), the model's QBO modulates high clouds such that colder UTLS temperatures in the model tend to have increased high cloud fraction. The correlation between monthly mean, tropically averaged model high cloud fraction and 100-hPa temperatures is -0.81 and is statistically significant across all ensemble members using a t test. Further, unlike SST patterns or the MJO-QBO link, the ensemble average high cloud change is in general consistent with the individual response of certain ensemble members. The consistency of this response suggests that QBO modulation of high clouds may not explain differences across ensemble members in any apparent MJO-QBO connection.

While the model QBO does change high clouds, zonal differences are evident across the ensemble in both high clouds and temperature. We hypothesize this is likely due in part to ENSO or differences in tropospheric processes linked to convection that might modulate these fields. However, correlation and composite analyses of whether changes in monthly high cloud amounts over the warm pool were linked to ensemble members' MJO activity changes in QBOE versus QBOW

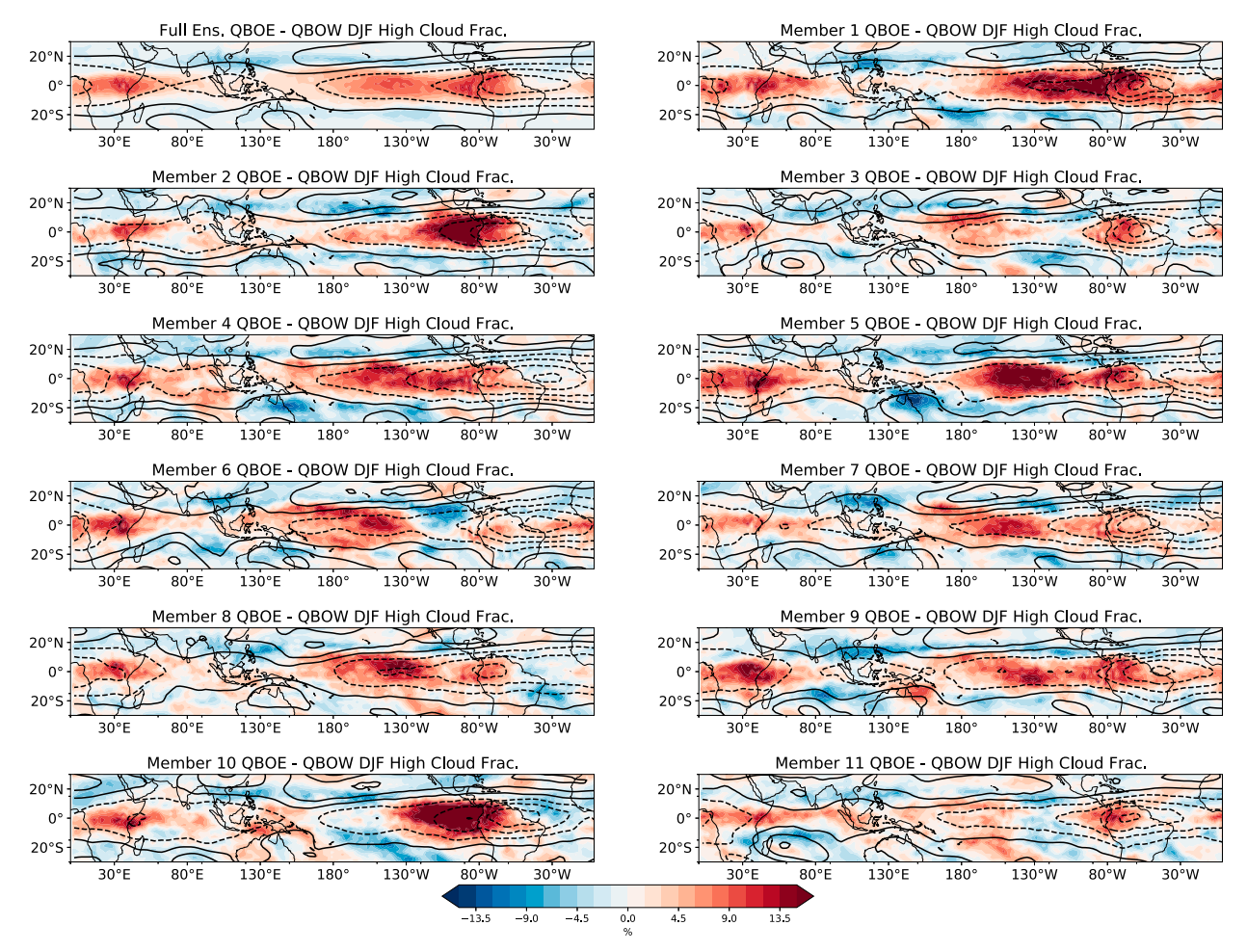


FIG. 12. The QBOE minus QBOW difference in the model high cloud fraction (shading) and 100-hPa temperatures (contours; from -2 to 2 K in 0.5-K intervals; negative dashed) during December–February for (top left) the full coupled ensemble and (bottom rows) individual ensemble members.

found no conclusive results. Thus, it is not clear whether the zonal asymmetries in high clouds are central to the lack of an MJO-QBO link, or whether they relate to the variability across the ensemble members' MJO-QBO connections.

Other high cloud biases that we did not examine could play a role in explaining the lack of a model MJO-QBO link. Notably, neither temperature anomalies nor high cloud changes in the model show strong QBOE-QBOW differences around the Maritime Continent or eastern Indian Ocean, whereas Son et al. (2017) observed clear high cloud differences associated with the QBO in this region (see their Fig. 8), and Tegtmeier et al. (2020) noted strong observed QBO temperature signals. Possible biases around the Maritime Continent in high clouds and upper tropospheric temperatures are consistent with convective biases in this region, all of which may be important if the Maritime Continent region is key to the observed MJO-QBO connection.

It is also possible that the radiative impacts of these high clouds and their influence on the MJO are not well simulated in the model. Because of the lack of any MJO–QBO signal in the model, and few observational benchmark studies in the literature against which to compare the model to, we have not conducted a more detailed analysis exploring this hypothesis. Finally, while we have explored the QBO impact on high clouds, the MJO also modulates high cirrus clouds in observations (Virts and Wallace 2014). As model daily high cloud data were not output, it is unclear whether the model MJO modulates high clouds in a manner consistent with observations. Yet if future observational work shows that MJO modulation of high clouds may be important, this could be explored further in models as another possible bias or missing process.

#### 4. Discussion

Deficiencies in the model-simulated MJO-QBO relationship could stem from one or more of four overlapping model issues: 1) errors in the simulated QBO, 2) errors in the simulated MJO, 3) errors in an unknown process(es) responsible for their coupling, or 4) the lack of an actual, physical MJO-QBO

connection in observations (implying that the observed relationship is a statistical fluke).

In this study, we have tried as much as possible to remove issues stemming from QBO biases by prescribing the QBO via nudging. This was inspired by the specific hypothesis put forth in the literature (e.g., Lee and Klingaman 2018; Hyemi Kim et al. 2020; Lim and Son 2020) that QBO biases in this region were central to models' lack of an MJO-QBO connection. Our results suggest that, to the extent that this model is representative, QBO biases are not the only reason why the MJO-QBO link is not simulated, although mean state biases in the stratosphere or the around the tropopause (e.g., Fig. 3) may still play a role. Note that while remedying QBO biases around the tropopause does not appear sufficient to capture an MJO-QBO link, it may still be necessary, insofar as both QBO and MJO processes in models likely need to be simulated with fidelity to capture the observed link.

Model MJO errors are more difficult to control. In section 3b, as well as the appendices, we noted that while the overall propagation, amplitude, and seasonal cycle of the MJO were well captured, the MJO showed several deficiencies in its vertical structure, and in the strength and location of convection, especially around the Maritime Continent. Model biases in 100-hPa temperatures associated with the MJO were also noted, although in several phases the cold-cap temperature signals in the model appeared comparable to observations. Still, any of these MJO simulation errors might contribute to the lack of an MJO–QBO link.

Aside from MJO biases, the model may miss some other key feature that is vital to the MJO-QBO relationship but not yet known. The model has a low vertical resolution, which could be detrimental in particular in regions like the UTLS. And GCMs in general have a horizontal resolution that requires the use of cumulus parameterizations, which recent cloud-resolving model studies (Back et al. 2020) have indicated may be important for explaining the lack of an MJO-QBO connection in models. The effect of both resolution and mean-state biases could be explored in future work. Several other pathways have been proposed for the MJO-QBO link, such as QBO changes to wave propagation or dynamics, QBO changes to the diurnal cycle over the Maritime Continent (Sun et al. 2019), or the effects of either the QBO (Son et al. 2017) or the MJO (Virts and Wallace 2014) on high clouds. In particular, we believe more detailed observational work that examines whether QBO or MJO modulation of high clouds could be useful in indicating whether this is indeed a viable pathway of influence, and could guide future modeling work to examine the representation of those processes in models.

Finally, the MJO-QBO link in observations may be due to chance: a statistical fluke made possible by the short observational record relative to the QBO time scale. Other processes unrelated to the stratosphere could explain some or all of the observed QBO's association with the MJO. Other features of the climate system such as tropical cyclones and ENSO have shown QBO-related "relationships" that change over long time scales (Garfinkel and Hartmann 2007; Camargo and Sobel 2010), which makes us question

whether these relationships are consequences of real stratospheric influence on the tropical troposphere. Yet we believe it is still premature to conclude that the MJO-QBO link found in observations is a fluke. The observed MJO-QBO link has passed stringent statistical tests, and is much stronger than anything our model experiments produce over an approximately four-decade span in many different ensemble members and sensitivity tests. Hyemi Kim et al. (2020) similarly found, looking across the CMIP6 models with internally generated QBOs, that the model spread in MJO-QBO connections did not produce a strong MJO-QBO link like that observed in any ensemble run of any model. This suggests that the observed link is significant, and is very unlikely to occur by chance. Both the MJO and the QBO are still difficult to simulate in GCMs, such that ultimately it is perhaps not surprising that modeling the interaction between these two phenomena is a stringent test that no GCM has yet passed.

### 5. Conclusions

We have examined the MJO-QBO relationship using a NASA GISS CMIP6-class coupled global climate model, Model E2.1 (Kelley et al. 2020). We carried out 11 ensemble experiments (which differ in their ocean initial conditions), each run for 37 years, and one control run that is run for 36 years. Additional sensitivity tests were also carried out, as shown in the appendices.

To include the QBO in the model, which otherwise does not possess one, the stratospheric zonal-mean zonal and meridional winds were nudged toward MERRA-2 reanalysis during the period from 1980-2017. This allows the model to simulate the QBO with relatively little bias (Figs. 1-3). While no nudging was applied to the model temperature, the thermal wind constraint leads to realistic simulation of QBO temperature anomalies, though the model mean state remains somewhat warmer ( $\sim$ 1.5 K) than observations at 100 hPa, with a more pronounced bias ( $\sim$ 1.9 K) in winter than summer. In all ensemble members the stratospheric state was nudged identically, and stratospheric differences across members are small. Compared to a control run without nudging, the nudged model shows changes in the troposphere when strong stratospheric changes are made, including changes in the tropical-mean zonal wind below 100 hPa (e.g., Fig. 1) and changes to tropical high cloud fraction in QBOE versus QBOW (Fig. 12). This suggests the model is sensitive to stratospheric changes (though perhaps in ways unrelated to the impact on the MJO).

In general, the model captures the MJO as well as or better than typical state-of-the art GCMs of this resolution (Figs. 4 and A1), although biases still remain. Importantly, we found biases in the strength of MJO convection, especially convection associated with the MJO around the Maritime Continent (Figs. 4 and 5), and the vertical structure of the coupled model's MJO (Fig. 6), which shows weaker than observed ascent and temperature anomalies in the upper troposphere, and a slightly more tilted vertical structure. The appendices demonstrate that the model captures approximately the correct MJO amplitude, viewed either with the RMM or OMI

TABLE B1. Measures of the MJO-QBO relationship in observations and the sensitivity experiments. The first column is the QBO change in MJO activity (measured by the warm pool averaged change in the standard deviation of OLR), and the second column is the correlation coefficient (*p* value in parentheses) between the MJO and QBO (see section 2a).

Data source	QBOE-QBOW MJO-OLR std dev	MJO-QBO correlation (p value)	
Observations	2.57	-0.59 (0.00)	
AMIP	0.19	0.22 (0.20)	
Grid-point nudging	-0.44	0.13 (0.46)	
30-min nudging time scale	0.23	0.31 (0.06)	
1-week nudging time scale	-0.53	-0.06(0.72)	
1-month nudging time scale	0.10	0.09 (0.60)	
Lower nudging transition region	0.08	0.25 (0.14)	
Higher nudging transition region	-0.71	0.09 (0.60)	
$1.5 \times \text{QBO}$	0.07	-0.04(0.81)	
$0.5 \times \text{QBO}$	-0.10	-0.10(0.57)	

index, and the MJO seasonal cycle, although OMI biases are still evident related to the seasonal cycle and the convective signature of the MJO.

We examined the MJO-QBO relationship using several metrics: the change in MJO amplitude in different QBO phases, the change in MJO-filtered OLR activity in different QBO phases, and the correlation of MJO and QBO indices. We focused our results on boreal winter and with the QBO defined at 50 hPa, but confirmed that our findings generalize to other seasons and QBO levels. Our main results can be summarized as follows:

- 1) No strong MJO-QBO link is evident in the nudged model. While some ensemble members do show stronger MJO events when the QBO is easterly versus westerly, no individual ensemble member shows a link consistently across all three MJO-QBO metrics in a way that seems to resemble observations (see Figs. 8-10). The full ensemble results analyzed together support the conclusion that no MJO-QBO link exists in the model.
- 2) Differences in the apparent MJO-QBO link in different ensemble members do not seem linked to SST variability or ENSO in a straightforward manner in the coupled model (e.g., Fig. 11), and the model further simulates qualitatively the observed link between the QBO and high cloud cover [an increase in high clouds during QBOE; see Fig. 12 and Son et al. (2017)]. The cause of the differences across the ensemble runs is not known, but is likely noise.
- 3) Sensitivity tests to the details of how nudging was implemented, including tests artificially increasing or decreasing the strength of the QBO by multiplying the winds by a factor of 0.5 or 1.5, do not show an MJO–QBO link (see Table B1 in appendix B). This suggests that our findings are not limited by the precise technical details of how the stratosphere was nudged.

This study suggests that model biases to the QBO, and in particular to QBO temperature anomalies in the lower stratosphere, are not responsible for the lack of an MJO–QBO link in this model. It is possible that the lack of an MJO–QBO link is due to biases simulating the structure of the MJO, the strength of MJO convective activity or mean-state convection around the warm pool, or some presently unknown mechanism important for the MJO–QBO link. In this regard more observational, theoretical, or modeling work on MJO dynamics and the MJO–OBO connection is much needed.

Acknowledgments. ZM, SW, and AS recognize support for this work by NSF AGS-1543932 and for ZM and AS by NASA Headquarters under the NASA Earth and Space Science Fellowship Program Grant 80NSSC18K1347. ZM further recognizes that this material was based upon work supported by the National Science Foundation under Award 2020305. CO thanks support from the NASA Modeling, Analysis and Prediction program, and resources provided by the NASA High-End Computing (HEC) Program through the NASA Center for Climate Simulation (NCCS) at Goddard Space Flight Center. Thanks to Isla Simpson, Elizabeth Barnes, and Chidong Zhang for feedback and guidance on early results from this work, and to three anonymous reviewers.

*Data availability statement.* Reanalysis datasets are publicly available at locations cited in the appropriate references.

The observed NOAA OLR data are available at https://psl.noaa.gov/data/gridded/data.interp\_OLR.html. The Hadley Centre sea surface temperature data set is available at https://www.metoffice.gov.uk/hadobs/hadisst/.

The observed RMM index is available at http://www.bom.gov.au/climate/mjo/graphics/rmm.74toRealtime.txt, the observed OMI index is available at https://www.esrl.noaa.gov/psd/mjo/mjoindex/omi.1x.txt, and the observed Niño-3.4 index is available at https://www.esrl.noaa.gov/psd/gcos\_wgsp/Timeseries/Data/nino34.long.data.

All data from the GCM experiments used in analysis or in preparing the figures discussed in this study are available via Zenodo at <a href="https://www.doi.org/10.5281/zenodo.4697457">https://www.doi.org/10.5281/zenodo.4697457</a>. Additional model output that was not analyzed in this study and is too large to be publicly archived is available from the corresponding author.

# APPENDIX A

### **Additional MJO Diagnostics**

In this appendix we present additional MJO diagnostics that, for length, were excluded from section 3b. These results focus on representation of the MJO in the model using the RMM and OMI index. Figure A1 shows the amplitude of OMI and RMM binned

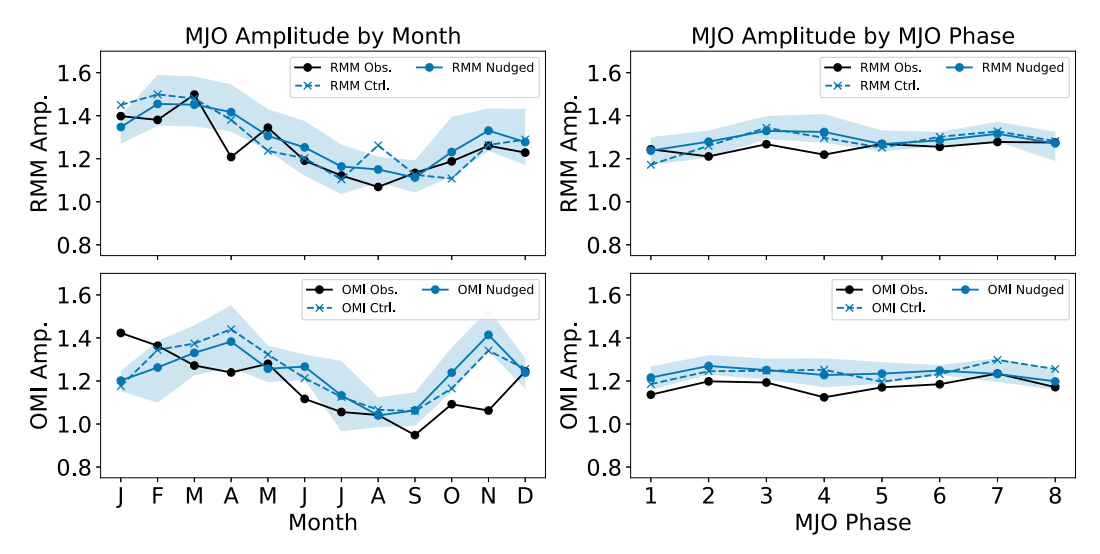


FIG. A1. MJO amplitude binned by (left) month and (right) MJO phase for observations (black) and the model (blue) for (top) the RMM index and (bottom) the OMI index. For nudged model runs, the solid blue line shows the ensemble mean and the shading shows the minimum and maximum value across the ensemble in each month/phase. The dashed blue line shows the control run.

by month (left) and MJO phase (right). Lines show the ensemble means, and the shading denotes the minimum and maximum for each month/phase across the ensemble members in the nudged model; also shown are the observed and control run values.

All model ensemble members and the control run capture the overall amplitude of RMM and OMI well. The model also shows fairly consistent amplitudes across different MJO phases, and the observations tend to be either in the range of the model ensemble, or just slightly below it. The observed MJO RMM seasonal cycle in observations is evident in both indices, with stronger events in Northern Hemisphere winter and weaker events in late summer and early fall; in summer the

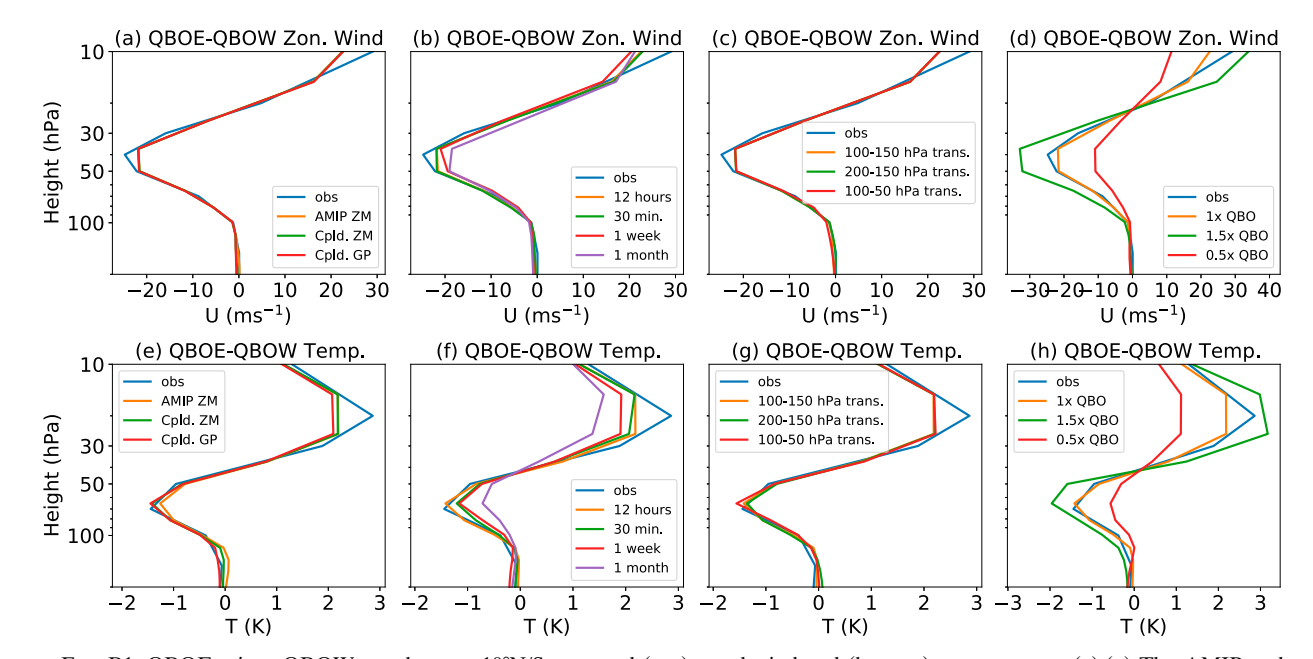


FIG. B1. QBOE minus QBOW zonal-mean,  $10^\circ N/S$  averaged (top) zonal wind and (bottom) temperatures. (a),(e) The AMIP and coupled ("Cpld.") model with zonal-mean nudging ("ZM") and grid-point nudging "GP". (b),(f) Changing the nudging time scale, as shown in the legend. (c),(g) The region over which the nudging is implemented, with no nudging below the region and full nudging above. (d),(h) Simulations with an artificially stronger or weaker QBO, as indicated (1  $\times$  QBO is the observed MERRA-2 winds). In some cases [e.g., in (a)] curves lie on top of each other, and only the last listed is apparent.

MJO is often referred to as the boreal summer intraseasonal oscillation (BSISO). Wang et al. (2018) showed that the OMI index better represents the BSISO in northern summer months. The model captures this seasonal cycle, though it looks better in RMM than in OMI. The only markedly different RMM month is April, when the observations dip lower than the model. In OMI, the models tend to be too strong in fall (e.g., September-November) and too weak in winter (e.g., January in particular). Capturing this seasonal cycle may be particularly important since the observed MJO-QBO link is limited to November-March, when the MJO is strongest (Yoo and Son 2016; Son et al. 2017; Abhik et al. 2019), although we do not diagnose what causes this seasonal difference between the model and observations. In general, in both RMM and OMI the coupled model is too strong in December and too weak in January/February.

In addition to the amplitude of the RMM and OMI indices, we also compared the autocorrelation of index amplitude and lag correlation between both indices' principal component time series. These provide measures, respectively, of how persistent the MJO is, and how coherent its propagation is in these two indices. The observed MJO amplitude autocorrelation drops to 1/e after 10 days for RMM and 22 days for OMI. The longer time scale of OMI is consistent with the smoother, more persistent nature of that index. In the model, the RMM index drops to below 1/e between 10 and 13 days across ensemble members, with an average of approximately 11 days. This indicates that the RMM is roughly as persistent in the model as observed. OMI in the model, however, shows more difference compared to observations: the model autocorrelation drops below 1/e between 12 and 21 days. This wide spread is due to the shape of the autocorrelation curve (not shown), which plateaus around 1/e such that small changes in the autocorrelation value about this threshold have a large impact on the precise day at which it is crossed. Still, the persistence of OMI in the model, unlike that of RMM, is markedly lower than in observation. We interpret this as indicating that, while MJO circulation anomalies captured by RMM are comparable in the model and observations, MJO convective signals tend to be less persistent in the model than observed (despite the fact that OMI as an index is more persistent than RMM in observations).

The lag correlation between the principal components of RMM and OMI shows similar behavior to that seen in the autocorrelations above. In observations, RMM2 lags RMM1 at a maximum of 9 days with a 0.56 correlation. In the model this value maximizes typically at 10 days with a correlation between 0.53 and 0.57, indicating the model MJO is roughly as coherent as observed when measured using RMM. The OMI values in the model show less coherence: the observations show that OMI2 lags OMI1 at a maximum of 10 days with a correlation of 0.72. In the model, the peak is typically around 9 or 10 days, but the correlation is lower, between 0.60 and 0.66. Similar to the conclusion from the autocorrelation analysis, this indicates that the coherence of MJO convective anomalies in

the model is lower than observed, while wind signals are better represented.

#### APPENDIX B

## **Sensitivity Tests**

In this appendix we show results from sensitivity tests to how the nudging was implemented. We examine sensitivity to the nudging time scale, the nudging vertical extent, whether zonalmean or grid-point nudging was implemented, and the target QBO winds we nudge to. We also briefly present results from one atmosphere-only ("AMIP") simulation. The AMIP model used here is also Model E2.1, but with prescribed SST and sea ice fraction (Rayner et al. 2003). The MJO in this simulation is markedly less realistic by many of the metrics we consider (not shown): the propagation and convection are both more biased compared to observations than in the coupled model. Thus, AMIP results are not presented in detail, and preliminary experiments looking at a larger ensemble of AMIP results confirmed the overall lack of an MJO–QBO link discussed below.

Figure B1 shows the QBOE minus QBOW wind and temperature from all of our sensitivity tests. Figures B1a and B1e show simulations changing whether zonal-mean or grid-point nudging is utilized, and from the AMIP run. The zonal-mean zonal wind is identical by design in the AMIP and coupled runs in the stratosphere where nudging is imposed. In the troposphere, the AMIP model shows larger biases in zonal-mean zonal wind in the tropics compared to the coupled run (not shown in detail). In the grid-point nudging, the zonal-mean wind is identical to the zonal-mean nudged run, although spatial patterns of zonal winds differ in the zonal-mean versus grid-point runs (and in the latter are close to observed; not shown). The temperature signals in the grid-point nudging do not differ substantially between the zonal-mean and grid-point nudging. In the AMIP run, overall temperature anomalies are slightly weaker, likely due to more substantial biases in the zonal wind structure in the upper troposphere in this run, as well as other mean-state biases.

Figures B1b and B1f show tests either shortening the nudging time scales to 30 minutes (the model time step) or extending it to one week or to one month. The changes are modest in general; the 30-min time scale shows winds that are largely identical to the 12-hourly time scale, while the 1-week and 1-month runs show increasingly weaker QBO wind signals, likely because the weaker forcing allows the model stratosphere to stay closer to the mean easterlies seen in the control. For reasons that are not clear, the QBO temperature signals are weaker when the nudging time scale is made shorter and when it is made longer than 12 h: both the 30-min and 1-week nudging time scales have temperature anomalies whose peak less than the 12-h nudging runs. The 1-month nudging runs show an even weaker temperature response, consistent with the weaker wind signals at upper levels.

Figures B1c and B1g show higher and lower transition regions over which the nudging occurs. Changes are generally not very large: the higher transition region shows some small differences in temperature, but overall the variability around the tropopause demonstrates small differences there. Figures B1d and B1h show the results from nudging to either an artificially

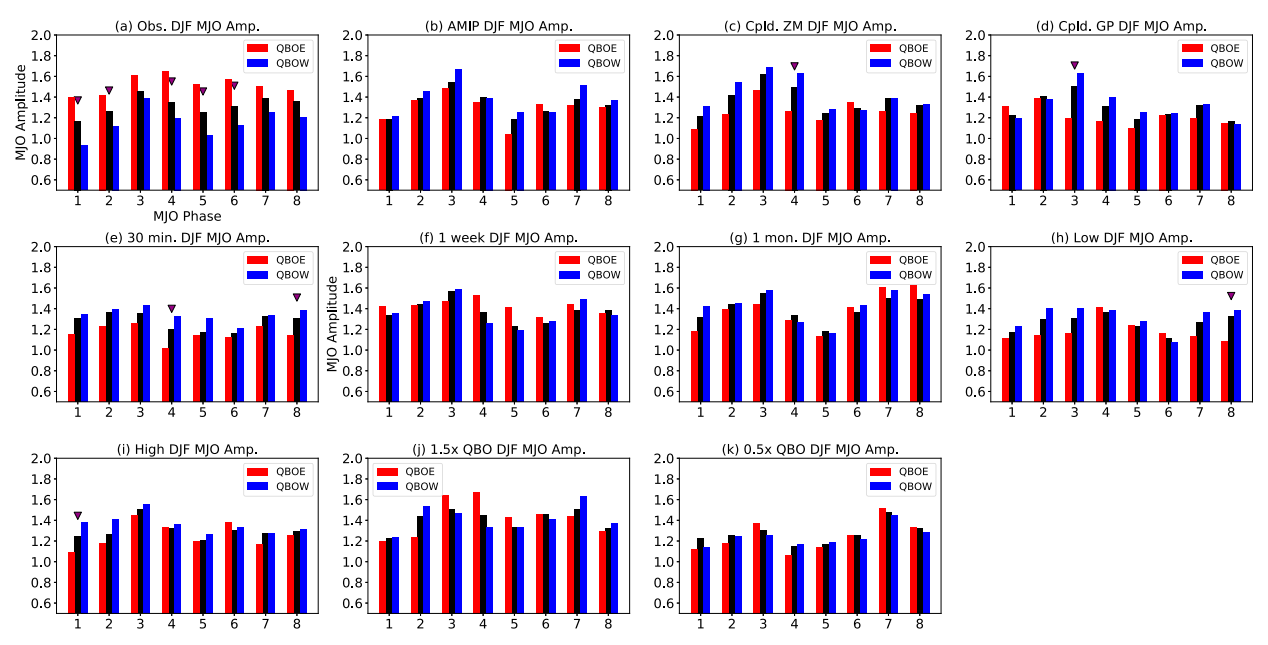


FIG. B2. As in Fig. 8, but showing the overall MJO amplitude in all DJF periods (black), QBOE months only (red), and QBOW months only (blue). Only RMM is shown; significance is denoted with a purple arrow. The names of the sensitivity test experiments are as described in the caption to Fig. B1, except "low" and "high," which refer to the 200–150- and 100–50-hPa nudging transitions experiments, respectively.

stronger or weaker QBO. This was done by multiplying the reanalysis stratospheric zonal and meridional winds by either a factor of 0.5 or 1.5 in the region in which nudging occurs. While it is a somewhat crude approach, our goal in these experiments was simply to explore whether making more drastic changes to the model stratosphere had an effect on the MJO. Wind and temperature signals associated with the QBO in these panels maintain their general structure, and the easterly to westerly transitions still occur at similar times as the observed QBO (not shown); the main effect is the amplitude change. In particular, the 1.5 times QBO runs show much stronger temperature signals both around 100 hPa and higher up around 70 hPa where the peak is, whereas the 0.5 QBO run shows clearly weaker QBO temperature anomalies.

While the wind and temperature anomalies associated with the QBO show changes both subtle and drastic across these experiments, none of the sensitivity experiments show a strong MJO–QBO relationship. Figure B2 shows similar MJO amplitude changes as in Fig. 8, but rather than the QBOE minus QBOW difference there we show the amplitude individually in QBOE, QBOW, and all winters. Also, here we use only RMM for simplicity. Table B1 further lists the warm pool MJO activity change and MJO–QBO correlation compared to observations.

None of the sensitivity tests show consistent MJO amplitude change across different QBO phases of the correct sign that appears significant; some show significance in one or two phases, but the sign of the change is not correct. If anything, in many phases the MJO seems stronger in QBOW than QBOE. Weak signals or signals of the opposite sign are further evident in Table B1: no runs show a large change in MJO activity over the warm pool, and most runs show no correlation. One run (with a 30-min time scale) shows a correlation coefficient of

0.31, which is almost significant at the 95% level, but is of the wrong sign compared to observations and therefore seems unlikely to be related to the observed MJO–QBO link.

The much stronger and weaker temperature and wind anomalies in the 1.5 times and 0.5 times QBO experiments also have no strong impact on the MJO that seems related to the observed MJO-QBO link. If anything the MJO looks stronger in QBOW in several of its phases in Fig. B1, and the relationship viewed by other metrics (Table B1) is both too weak and often of the opposite sign to what is observed. The fact that making these large and unrealistic changes to the stratospheric winds has only a marginal impact on the MJO makes it very unlikely that the inability of this model to show an MJO-QBO relationship is linked to something as subtle as the precise amplitude of tropopause layer QBO temperature anomalies. Taken as a whole, the results in this appendix suggest that the nudging parameters and implementation, as well as the coupled versus AMIP versions of the model and the strength of the target QBO winds to which we nudge, are not crucial to the model's failure to show an MJO-QBO relationship.

#### REFERENCES

Abhik, S., and H. H. Hendon, 2019: Influence of the QBO on the MJO during coupled model multiweek forecasts. *Geophys. Res. Lett.*, **46**, 9213–9221, https://doi.org/10.1029/2019GL083152.

—, —, and M. C. Wheeler, 2019: On the sensitivity of convectively coupled equatorial waves to the quasi-biennial oscillation. *J. Climate*, 32, 5833–5847, https://doi.org/10.1175/JCLI-D-19-0010.1.

Back, S.-Y., J.-Y. Han, and S.-W. Son, 2020: Modeling evidence of QBO-MJO connection: A case study. *Geophys. Res. Lett.*, 47, e2020GL089480, https://doi.org/10.1029/2020GL089480.

- Baldwin, M. P., and Coauthors, 2001: The quasi-biennial oscillation. *Rev. Geophys.*, **39**, 179–229, https://doi.org/10.1029/1999RG000073.
- Bauer, S. E., A. Ault, and K. A. Prather, 2013: Evaluation of aerosol mixing state classes in the GISS ModelE-MATRIX climate model using single-particle mass spectrometry measurements. J. Geophys. Res. Atmos., 118, 9834–9844, https://doi.org/10.1002/jgrd.50700.
- Camargo, S. J., and A. H. Sobel, 2010: Revisiting the influence of the quasi-biennial oscillation on tropical cyclone activity. *J. Climate*, 23, 5810–5825, https://doi.org/10.1175/2010JCLI3575.1.
- Christiansen, B., S. Yang, and M. S. Madsen, 2016: Do strong warm ENSO events control the phase of the stratospheric QBO? *Geophys. Res. Lett.*, 43, 10489–10495, https://doi.org/10.1002/2016GL070751.
- Collimore, C. C., D. W. Martin, M. H. Hitchman, A. Huesmann, and D. E. Waliser, 2003: On the relationship between the QBO and tropical deep convection. *J. Climate*, 16, 2552–2568, https://doi.org/ 10.1175/1520-0442(2003)016<2552:OTRBTQ>2.0.CO;2.
- Coy, L., K. Wargan, A. M. Molod, W. R. McCarty, and S. Pawson, 2016: Structure and dynamics of the quasi-biennial oscillation in MERRA-2. J. Climate, 29, 5339–5354, https://doi.org/10.1175/JCLI-D-15-0809.1.
- Densmore, C. R., E. R. Sanabia, and B. S. Barrett, 2019: QBO influence on MJO amplitude over the Maritime Continent: Physical mechanisms and seasonality. *Mon. Wea. Rev.*, 147, 389–406, https://doi.org/10.1175/MWR-D-18-0158.1.
- Domeisen, D. I., C. I. Garfinkel, and A. H. Butler, 2019: The teleconnection of El Niño Southern Oscillation to the stratosphere. *Rev. Geophys.*, 57, 5–47, https://doi.org/10.1029/2018RG000596.
- Eyring, V., S. Bony, G. A. Meehl, C. A. Senior, B. Stevens, R. J. Stouffer, and K. E. Taylor, 2016: Overview of the Coupled Model Intercomparison Project phase 6 (CMIP6) experimental design and organization. *Geosci. Model Dev.*, 9, 1937–1958, https://doi.org/10.5194/gmd-9-1937-2016.
- Ferranti, L., T. N. Palmer, F. Molteni, and E. Klinker, 1990: Tropical–extratropical interaction associated with the 30–60 day oscillation and its impact on medium and extended range prediction. *J. Atmos. Sci.*, **47**, 2177–2199, https://doi.org/10.1175/1520-0469(1990)047<2177:TEIAWT>2.0.CO;2.
- Garfinkel, C. I., and D. L. Hartmann, 2007: Effects of the El Niño– Southern Oscillation and the quasi-biennial oscillation on polar temperatures in the stratosphere. J. Geophys. Res., 112, D19112, https://doi.org/10.1029/2007JD008481.
- Gelaro, R., and Coauthors, 2017: The Modern-Era Retrospective Analysis for Research and Applications, version 2 (MERRA-2). J. Climate, 30, 5419–5454, https://doi.org/10.1175/JCLI-D-16-0758.1.
- Gill, A. E., 1980: Some simple solutions for heat-induced tropical circulation. *Quart. J. Roy. Meteor. Soc.*, **106**, 447–462, https:// doi.org/10.1002/qj.49710644905.
- Henderson, S. A., and E. D. Maloney, 2018: The impact of the Madden–Julian oscillation on high-latitude winter blocking during El Niño–Southern Oscillation events. *J. Climate*, 31, 5293–5318, https://doi.org/10.1175/JCLI-D-17-0721.1.
- —, and E. A. Barnes, 2016: The influence of the Madden–Julian oscillation on Northern Hemisphere winter blocking. *J. Climate*, 29, 4597–4616, https://doi.org/10.1175/JCLI-D-15-0502.1.
- Hendon, H. H., and S. Abhik, 2018: Differences in vertical structure of the Madden–Julian oscillation associated with the quasi-biennial oscillation. *Geophys. Res. Lett.*, 45, 4419–4428, https://doi.org/10.1029/2018GL077207.
- Hersbach, H., and Coauthors, 2020: The ERA5 global reanalysis. *Quart. J. Roy. Meteor. Soc.*, **146**, 1999–2049, https://doi.org/10.1002/qj.3803.
- Holloway, C. E., and J. D. Neelin, 2007: The convective cold top and quasi equilibrium. J. Atmos. Sci., 64, 1467–1487, https:// doi.org/10.1175/JAS3907.1.

- Holton, J. R., and R. S. Lindzen, 1972: An updated theory for the quasi-biennial cycle of the tropical stratosphere. *J. Atmos. Sci.*, **29**, 1076–1080, https://doi.org/10.1175/1520-0469(1972) 029<1076:AUTFTQ>2.0.CO;2.
- Hood, L. L., 2017: QBO/solar modulation of the boreal winter Madden–Julian oscillation: A prediction for the coming solar minimum. *Geophys. Res. Lett.*, 44, 3849–3857, https://doi.org/ 10.1002/2017GL072832.
- Jeuken, A., P. Siegmund, L. Heijboer, J. Feichter, and L. Bengtsson, 1996: On the potential of assimilating meteorological analyses in a global climate model for the purpose of model validation. J. Geophys. Res., 101, 16 939–16 950, https:// doi.org/10.1029/96JD01218.
- Jiang, X., and Coauthors, 2020: Fifty years of research on the Madden–Julian oscillation: Recent progress, challenges, and perspectives. J. Geophys. Res. Atmos., 125, e2019JD030911, https://doi.org/10.1029/2019JD030911.
- Kelley, M., and Coauthors, 2020: GISS-E2.1: Configurations and climatology. *J. Adv. Model. Earth Syst.*, **12**, e2019MS002025, https://doi.org/10.1029/2019MS002025.
- Kiladis, G. N., J. Dias, K. H. Straub, M. C. Wheeler, S. N. Tulich, K. Kikuchi, K. M. Weickmann, and M. J. Ventrice, 2014: A comparison of OLR and circulation-based indices for tracking the MJO. *Mon. Wea. Rev.*, 142, 1697–1715, https://doi.org/ 10.1175/MWR-D-13-00301.1.
- Kim, D., A. H. Sobel, A. D. Del Genio, Y. Chen, S. J. Camargo, M.-S. Yao, M. Kelley, and L. Nazarenko, 2012: The tropical subseasonal variability simulated in the NASA GISS general circulation model. *J. Climate*, 25, 4641–4659, https://doi.org/ 10.1175/JCLI-D-11-00447.1.
- Kim, Hera, S.-W. Son, and C. Yoo, 2020: QBO modulation of the MJO-related precipitation in East Asia. *J. Geophys. Res. Atmos.*, 125, e2019JD031929, https://doi.org/10.1029/2019JD031929.
- Kim, Hyemi, J. H. Richter, and Z. Martin, 2019: Insignificant QBO–MJO prediction skill relationship in the SubX and S2S subseasonal reforecasts. J. Geophys. Res. Atmos., 124, 12 655– 12 666, https://doi.org/10.1029/2019JD031416.
- —, J. M. Caron, J. H. Richter, and I. R. Simpson, 2020: The lack of QBO–MJO connection in CMIP6 models. *Geophys. Res. Lett.*, 47, e2020GL087295, https://doi.org/10.1029/2020GL087295.
- Klotzbach, P., S. Abhik, H. Hendon, M. Bell, C. Lucas, A. Marshall, and E. Oliver, 2019: On the emerging relationship between the stratospheric quasi-biennial oscillation and the Madden–Julian oscillation. Sci. Rep., 9, 2981, https:// doi.org/10.1038/s41598-019-40034-6.
- Lee, J. C., and N. P. Klingaman, 2018: The effect of the quasibiennial oscillation on the Madden–Julian oscillation in the Met Office Unified Model global ocean mixed layer configuration. *Atmos. Sci. Lett.*, **19**, e816, https://doi.org/10.1002/asl.816.
- Liebmann, B., and C. A. Smith, 1996: Description of a complete (interpolated) outgoing longwave radiation dataset. *Bull. Amer. Meteor. Soc.*, 77, 1275–1277.
- Lim, Y., and S.-W. Son, 2020: QBO–MJO connection in CMIP5 models. J. Geophys. Res. Atmos., 125, e2019JD032157, https://doi.org/10.1029/2019JD032157.
- —, —, A. G. Marshall, H. H. Hendon, and K.-H. Seo, 2019: Influence of the QBO on MJO prediction skill in the subseasonal-to-seasonal prediction models. *Climate Dyn.*, 53, 1681–1695, https://doi.org/10.1007/s00382-019-04719-y.
- Lindzen, R. S., and J. R. Holton, 1968: A theory of the quasi-biennial oscillation. *J. Atmos. Sci.*, **25**, 1095–1107, https://doi.org/10.1175/1520-0469(1968)025<1095:ATOTQB>2.0.CO;2.

- Madden, R. A., and P. R. Julian, 1971: Detection of a 40–50 day oscillation in the zonal wind in the tropical Pacific. *J. Atmos. Sci.*, 28, 702–708, https://doi.org/10.1175/1520-0469(1971)028<0702: DOADOI>2.0.CO;2.
- —, and —, 1972: Description of global-scale circulation cells in the tropics with a 40–50 day period. *J. Atmos. Sci.*, **29**, 1109–1123, https://doi.org/10.1175/1520-0469(1972)029<1109: DOGSCC>2.0.CO;2.
- Marshall, A. G., H. H. Hendon, S.-W. Son, and Y. Lim, 2017: Impact of the quasi-biennial oscillation on predictability of the Madden–Julian oscillation. *Climate Dyn.*, 49, 1365–1377, https://doi.org/10.1007/s00382-016-3392-0.
- Martin, Z., S. Wang, J. Nie, and A. Sobel, 2019: The impact of the QBO on MJO convection in cloud-resolving simulations. J. Atmos. Sci., 76, 669–688, https://doi.org/10.1175/JAS-D-18-0179.1
- —, F. Vitart, S. Wang, and A. Sobel, 2020: The impact of the stratosphere on the MJO in a forecast model. *J. Geophys. Res. Atmos.*, **125**, e2019JD032106, https://doi.org/10.1029/ 2019JD032106.
- Matsuno, T., 1966: Quasi-geostrophic motions in the equatorial area. *J. Meteor. Soc. Japan*, **44**, 25–43, https://doi.org/10.2151/jmsj1965.44.1\_25.
- Mayer, K. J., and E. A. Barnes, 2020: Subseasonal midlatitude prediction skill following quasi-biennial oscillation and Madden–Julian Oscillation activity. Wea. Climate Dyn., 1, 247–259, https://doi.org/10.5194/wcd-1-247-2020.
- Mundhenk, B. D., E. A. Barnes, E. D. Maloney, and C. F. Baggett, 2018: Skillful empirical subseasonal prediction of landfalling atmospheric river activity using the Madden–Julian oscillation and quasi-biennial oscillation. *npj Climate Atmos. Sci.*, 1, 20177, https://doi.org/10.1038/s41612-017-0008-2.
- Nie, J., and A. H. Sobel, 2015: Responses of tropical deep convection to the QBO: Cloud-resolving simulations. *J. Atmos. Sci.*, 72, 3625–3638, https://doi.org/10.1175/JAS-D-15-0035.1.
- Nishimoto, E., and S. Yoden, 2017: Influence of the stratospheric quasi-biennial oscillation on the Madden–Julian oscillation during austral summer. J. Atmos. Sci., 74, 1105–1125, https:// doi.org/10.1175/JAS-D-16-0205.1.
- Rayner, N., D. E. Parker, E. Horton, C. K. Folland, L. V. Alexander, D. Rowell, E. Kent, and A. Kaplan, 2003: Global analyses of sea surface temperature, sea ice, and night marine air temperature since the late nineteenth century. *J. Geophys. Res.*, 108, 4407, https://doi.org/10.1029/2002JD002670.
- Richter, J. H., J. A. Anstey, N. Butchart, Y. Kawatani, G. A. Meehl, S. Osprey, and I. R. Simpson, 2020: Progress in simulating the quasi-biennial oscillation in CMIP models. *J. Geophys. Res. Atmos.*, 125, e2019JD032362, https://doi.org/10.1029/2019JD032362.
- Rind, D., and Coauthors, 2020: GISS Model E2.2: A climate model optimized for the middle atmosphere—Model structure, climatology, variability, and climate sensitivity. *J. Geophys. Res. Atmos.*, 125, e2019JD032204, https://doi.org/10.1029/2019JD032204.
- Sakaeda, N., J. Dias, and G. N. Kiladis, 2020: The unique characteristics and potential mechanisms of the MJO–QBO relationship. J. Geophys. Res. Atmos., 125, e2020JD033196, https://doi.org/10.1029/2020JD033196.
- Schmidt, G. A., and Coauthors, 2014: Configuration and assessment of the GISS ModelE2 contributions to the CMIP5 archive. J. Adv. Model. Earth Syst., 6, 141–184, https://doi.org/10.1002/2013MS000265.

- Shindell, D., and Coauthors, 2013: Interactive ozone and methane chemistry in GISS-E2 historical and future climate simulations. *Atmos. Chem. Phys.*, 13, 2653–2689, https://doi.org/ 10.5194/acp-13-2653-2013.
- Son, S.-W., Y. Lim, C. Yoo, H. H. Hendon, and J. Kim, 2017: Stratospheric control of the Madden–Julian oscillation. J. Climate, 30, 1909–1922, https://doi.org/10.1175/JCLI-D-16-0620.1
- Stan, C., D. M. Straus, J. S. Frederiksen, H. Lin, E. D. Maloney, and C. Schumacher, 2017: Review of tropical–extratropical teleconnections on intraseasonal time scales. *Rev. Geophys.*, 55, 902–937, https://doi.org/10.1002/2016RG000538.
- Sun, L., H. Wang, and F. Liu, 2019: Combined effect of the QBO and ENSO on the MJO. *Atmos. Oceanic Sci. Lett.*, **12**, 170–176, https://doi.org/10.1080/16742834.2019.1588064.
- Tegtmeier, S., J. Anstey, S. Davis, I. Ivanciu, Y. Jia, D. McPhee, and R. Pilch Kedzierski, 2020: Zonal asymmetry of the QBO temperature signal in the tropical tropopause region. *Geophys. Res. Lett.*, 47, e2020GL089533, https://doi.org/10.1029/2020GL089533.
- Toms, B. A., E. A. Barnes, E. D. Maloney, and S. C. van den Heever, 2020: The global teleconnection signature of the Madden–Julian oscillation and its modulation by the quasi-biennial oscillation. J. Geophys. Res. Atmos., 125, e2020JD032653, https:// doi.org/10.1029/2020JD032653.
- Virts, K. S., and J. M. Wallace, 2014: Observations of temperature, wind, cirrus, and trace gases in the tropical tropopause transition layer during the MJO. J. Atmos. Sci., 71, 1143–1157, https://doi.org/10.1175/JAS-D-13-0178.1.
- Vitart, F., 2017: Madden—Julian oscillation prediction and teleconnections in the S2S database. *Quart. J. Roy. Meteor. Soc.*, 143, 2210–2220, https://doi.org/10.1002/qj.3079.
- —, and Coauthors, 2017: The Subseasonal to Seasonal (S2S) prediction project database. *Bull. Amer. Meteor. Soc.*, 98, 163–173, https://doi.org/10.1175/BAMS-D-16-0017.1.
- Wang, S., 2020: A precipitation-based index for tropical intraseasonal oscillations. *J. Climate*, 33, 805–823, https://doi.org/ 10.1175/JCLI-D-19-0019.1.
- —, D. Ma, A. H. Sobel, and M. K. Tippett, 2018: Propagation characteristics of BSISO indices. *Geophys. Res. Lett.*, 45, 9934–9943, https://doi.org/10.1029/2018GL078321.
- —, M. K. Tippett, A. H. Sobel, Z. K. Martin, and F. Vitart, 2019: Impact of the QBO on prediction and predictability of the MJO convection. *J. Geophys. Res. Atmos.*, **124**, 11 766–11 782, https://doi.org/10.1029/2019JD030575.
- Wheeler, M. C., and G. N. Kiladis, 1999: Convectively coupled equatorial waves: Analysis of clouds and temperature in the wavenumber–frequency domain. J. Atmos. Sci., 56, 374–399, https://doi.org/10.1175/1520-0469(1999)056<0374:CCEWAO>2.0.CO;2.
- ——, and H. H. Hendon, 2004: An all-season real-time multivariate MJO index: Development of an index for monitoring and prediction. *Mon. Wea. Rev.*, **132**, 1917–1932, https://doi.org/10.1175/1520-0493(2004)132<1917:AARMMI>2.0.CO;2.
- Yoo, C., and S.-W. Son, 2016: Modulation of the boreal wintertime Madden–Julian oscillation by the stratospheric quasi-biennial oscillation. *Geophys. Res. Lett.*, 43, 1392–1398, https://doi.org/ 10.1002/2016GL067762.
- Zhang, C., 2005: Madden–Julian oscillation. Rev. Geophys., 43, RG2003, https://doi.org/10.1029/2004RG000158.
- ——, and B. Zhang, 2018: QBO–MJO connection. *J. Geophys. Res. Atmos.*, **123**, 2957–2967, https://doi.org/10.1002/2017JD028171.